ChemSusChem

Research Article
doi.org/10.1002/cssc.202400331

Chemistry Europe
European Chemical Societies Publishing

www.chemsuschem.org

A General and Highly Versatile Heterogeneous Pd-Catalyzed Oxidative Aminocarbonylation of Alkynes with Aromatic and Aliphatic Amines

Juan Camilo Arango-Daza,[a] Jose R. Cabrero-Antonino,*[a] and Rosa Adam*[b]

An efficient heterogeneous catalytic system for the oxidative aminocarbonylation of alkynes and amines in the presence of CO/O_2 to afford substituted propiolamides has been developed. The active nanocatalyst, [Pd/Mg_3Al-LDH]-300(D), is composed by Pd nanoaggregates (2–3 nm average particle size) stabilized over a partially dehydrated [Mg_3Al-LDH] matrix. The methodology has resulted widely applicable, being the first catalytic system, either homogeneous or heterogeneous, able to activate not only aliphatic amines but also poorly-nucleophilic aromatic amines. In fact, >60 substituted propiolamides have been synthesized in good to excellent isolated yields through this methodology, being 27 novel compounds. An important characterization effort (XRD, ^{27}Al MAS NMR, TGA, TPD-CO_2, BET area, XPS, HAADF-HRSTEM and HRTEM) and optimization of the synthesis conditions of the optimal catalyst has been performed. This study, together with a series of kinetic and mechanistic essays, indicates that the optimal catalyst is composed by Pd(0) species stabilized in a partially dehydrated/dehydroxylated LDH material with a Mg/Al molar ratio of 3 and a small crystallite size. All the experimental data indicates that the *in situ* formation of [PdI_2] active species in the material surface together with the presence of a matrix with the optimal acid/base properties are key aspects of this process.

Introduction

During the last years, the development of oxidative couplings involving the activation of C–H bonds has become a feasible and attractive methodology in organic chemistry.[1–5] In this respect, the synthesis of a structural diversity of carbonyl compounds through the introduction of easily available carbon monoxide in these cross-coupling protocols has been achieved. Thus, oxidative carbonylation reactions are convenient strategies employing two nucleophiles, a CO source and a suitable oxidant.[6–8] Obviously, these methodologies are advantageous when unfunctionalized nucleophiles are employed in the presence of molecular oxygen as oxidant.[9] Owing to its interest, a myriad of mainly homogeneous catalytic systems based on Pd has been developed. Hence, the design and study of alternative heterogeneous catalysts able to mediate these interesting transformations is an important goal that can potentially increase the sustainability of these reactions.

N,3-Substituted propiolamides, also known as alk-2-ynamides, are a specific type of carbonyl compounds with relevant biological activities. For example, compounds bearing the propiolamide scaffold have been described to present activities as inhibitors of enzymes such as matrix metalloproteinases[10] or Nek2 kinases,[11] with potential uses as drugs for the treatment of cancer, atherosclerosis or arthritis. In addition, this class of compounds are highly versatile intermediates in the synthesis of heterocycles bearing a lactam or cyclic carbamate moiety in their structure (Scheme 1, A). In fact, butyrolactams,[12] spirolactams,[13–14] benzapines,[15] oxazolidinones,[16] quinolinones,[13] oxindoles[17–18] and pyrroloindolones[19] have been accessed from the corresponding alkynamides. Considering the great potential of heterocycles as biological active compounds, the cyclization of propiolamides is an interesting approach that has been already applied for accessing to relevant compounds. In fact, an oxindole based molecule with adenosine 5′-monophosphate-activated protein kinase (AMPK) activator activity has been accessed through this methodology and applied as antidiabetic drug (Scheme 1, A).[18] Obviously, the potential of obtaining a high structural diversity of heterocycles from these cyclizations is significantly enlarged with the structural diversity of the corresponding propiolamide. Hence, the development of oxidative carbonylation protocols that tolerate a large structural diversity of amines and alkynes to obtain these interesting precursors has a high synthetic interest.

Due to the large relevance of propiolamides, several synthetic strategies have been developed recently for their preparation including non-catalytic methodologies[20–27] that,

[a] Dr. J. C. Arango-Daza, Dr. J. R. Cabrero-Antonino
Instituto de Tecnología Química
Universitat Politécnica de València-Consejo Superior Investigaciones Científicas (UPV-CSIC)
Avda. de los Naranjos s/n, 46022, València (Spain)
E-mail: jcabrero@itq.upv.es

[b] Dr. R. Adam
Departament de Química Orgànica, Facultat de Farmàcia
Universitat de València
Av. Vicent Andrés Estellés s/n, 46100, Burjassot, València (Spain)
E-mail: rosa.adam@uv.es

Supporting information for this article is available on the WWW under https://doi.org/10.1002/cssc.202400331

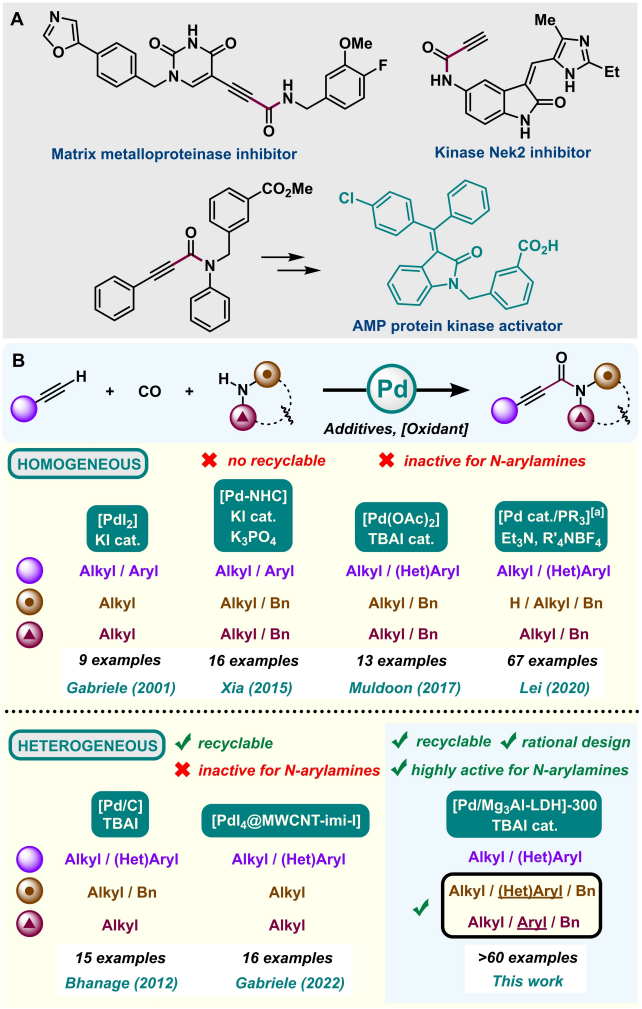

Scheme 1. (A) Some examples of biological active propiolamides or propiolamides acting as precursors of bioactive molecules. (B) Pd-catalyzed oxidative aminocarbonylation of terminal alkynes with 1° or 2° amines for the direct production of *N*,3-substituted propiolamides (reported examples and this work). [a] Electrochemical protocol. [Pd-NHC] = [*i*Pr–Pd-Peppsi-Cl_2]. NHC = *N*-Heterocyclic carbene. TBAI = Tetrabuthylammonium iodide. [Pd] cat. = [$PdCl_2$] or [$Pd(PPh_3)Cl_2$]. [PR_3] = [P(*p*-tol)$_3$] or [PPh_3]. R′ = Et or *n*-Bu. [MWCNT-imi-I] = multi-walled carbon nanotubes-imidazol based poly ionic liquid iodide network. AMP = Adenosine 5′-monophosphate.

although can be practical, are not efficient from the viewpoint of atom economy. Regarding catalytic methods, protocols employing amide-based compounds,[28–32] isocyanates[33] or isocyanides[34–35] have been also explored in the presence of homogeneous catalytic systems. In addition, several photocatalytic processes[36–39] or catalytic methodologies involving pre-functionalized alkynes[40–42] have been reported. The straightforward synthesis of alkynamides through oxidative carbonylation protocols starting from an alkyne, an amine and CO/O_2 has awaken a large interest in the last years. Among these works, several homogeneous methods have been published such as the pioneer example reported by Salerno and Gabriele in 2001 based on [PdI_2] (Scheme 1, B).[43] Since then, other Pd homogeneous systems have been published by the groups of Xia,[44] Muldoon[45] and Lei[46] (Scheme 1, B). This last example is especially interesting as the authors employed an electrochemical approach to perform the reoxidation of the Pd system, and the protocol worked with primary amines. Up to date, only two methodologies employing heterogeneous reusable catalytic systems have been reported by the groups of Bhanage[47] and Gabriele[48] (Scheme 1, B). Furthermore, it is important to highlight that none of these methods, neither homogeneous nor heterogeneous, was able to catalyze the oxidative carbonylation of alkynes with aromatic amines. This is an important limitation of the currently described oxidative carbonylation protocols for the synthesis of propiolamides, owing the large relevance of *N*-aryl based propiolamides as compounds with biological activity or intermediates.

The rational design and development of novel catalytic nanomaterials which fulfill the requirements of demanding chemical transformations is a hot topic in catalysis.[49–52] As it has been exposed, designing an active, selective and reusable catalytic system able to activate the poorly nucleophilic (hetero)aryl amines towards their oxidative carbonylation with alkynes is of current interest. A careful analysis of the proposed reaction mechanisms for this transformation[43,46] clearly suggests that a Pd species is needed together with basic centers assisting the amine and alkyne deprotonation. In fact, all the described catalytic systems, either homogeneous or heterogeneous, are based on Pd. However, in contrast with what occurs with the Buchwald-Hartwig amination,[53–54] not all the described protocols for the oxidative aminocarbonylation of alkynes employ a basic additive or catalyst, due to the different nature of this oxidative process. Despite the lower basicity of *N*-aryl amines in comparison with *N*-alkyl amines,[55–56] our hypothesis here is that a material with basic centers could facilitate their deprotonation and, hence, their conversion in better nucleophiles able to undergo the process of interest.

Layered double hydroxides (LDHs) are a class of laminated 2D materials with basic properties based on brucite [$Mg(OH)_2$]-like layers in which some divalent cations have been replaced by trivalent ones.[57–60] These nanostructured solids present positively charged sheets, whose charge is balanced by the presence of anions in the hydrated interlayer. A general formula for LDHs would be $[M^{2+}_{1-x}M^{3+}_{x}(OH)_2]^{x+}(A^{n-})_{x/n}\cdot yH_2O$, in which the most common M^{2+} is Mg^{2+} and M^{3+} is Al^{3+}, while the anion is usually CO_3^{2-}. The most employed LDH material is the commercially available hydrotalcite (HT) with the formula $[Mg_6Al_2(OH)_{16}CO_3\cdot 4H_2O]$. Structurally, each Mg^{2+} is coordinated with six different OH^- groups in an octahedral distribution and shares edges with neighboring Mg^{2+} or Al^{3+} atoms to create 2D sheets. The presence of such hydroxide layers as well as the intercalating anions confer LDHs surface with special Brönsted basic features. Interestingly, LDHs basicity can be easily tuned through several strategies such as the modification of the molar ratio composition (M^{2+}/M^{3+}) and/or the nature of M^{2+}, M^{3+} and the exchangeable interlayer anion (A^{n-}).[58,60] Moreover, a controlled thermal treatment of LDHs at $T > 450\,°C$ produces the corresponding derived mixed metal oxide (MMO), with interesting properties such as a Lewis basic character and larger surface areas.[58,61] Hence, due to the modulable basicity of LDHs and their corresponding MMO derivatives, these materials have

been intensively studied for various applications in the last years (catalysis, polymer science, drug delivery, etc).[57–60,62–64] Among these applications, their employment as supports of metal species for their use as reusable catalysts in organic synthesis is especially interesting.[60,65–68]

Hence, in this work we have performed the design of an active and reusable material with catalytic activity for the oxidative aminocarbonylation of alkynes and amines, including for the first time (hetero)aryl amines. To this end, we have explored the activity of several materials based on Pd nanoparticles over a matrix with basic properties, mainly of LDH or derived mixed metal oxide nature. An important effort has been done to find the most active material putting an especial emphasis in the modulation of the basic properties of the matrix and the Pd oxidation state.

Results and Discussion

As a starting point of our investigation, we selected as benchmark reaction the aminocarbonylation of phenylacetylene **1** with *N*-methylaniline **2**, as a representative example of aromatic amine with a relatively low nucleophilicity, in the presence of a CO/O_2 mixture (15/5 bar), tetrabuthylamonium iodide (TBAI) as an additive and EtOAc as solvent at 100 °C.

Then, a series of materials were designed as potential catalysts for this transformation based on Pd nanoparticles, active to mediate carbonylative couplings, stabilized over basic matrices, in principle able to activate poorly nucleophilic aromatic amines. The materials were synthesized at 1.5 wt% of Pd and pyrolized at 500 °C. To our delight, all the materials containing Pd nanoparticles over basic supports presented some activity as catalysts in this reaction (Table 1, entries 1–6). In the case of materials employing matrices such as $[La_2O_3]$ or spinel, $[MgAl_2O_4]$, low yields of the propiolamide **3** were obtained (9–26%, Table 1, entries 1 and 5), whereas materials with [MgO], $[CeO_2]$ or $[Al_2O_3]$ as supports afforded **3** in good yields (52–67%, Table 1, entries 2–4). Remarkably, the best yield of **3** was obtained with $[Pd/Mg_3Al\text{-}LDH]$-500 as catalyst, a material synthesized employing a LDH with a Mg/Al ratio of 3 as support (88%, Table 1, entry 6). Here it is important to remark that, after a pyrolysis treatment of the corresponding LDH at 500 °C, the structure of this catalyst corresponds to an LDH-derived metal mixed oxide (MMO), as it will be demonstrated next through several characterization techniques (*vide infra*, Figure 1 and Figure S8). In the absence of Pd, the corresponding LDH-derived MMO matrix, $[Mg_3Al\text{-}LDH]$-500, showed no catalytic activity for the aminocarbonylation (Table 1, entry 8), whereas a homogeneous Pd salt such as $[Pd(acac)_2]$ resulted to be a significant less active catalyst for this transformation (Table 1, entry 7).

At this point, an optimization of the reaction parameters employing $[Pd/Mg_3Al\text{-}LDH]$-500 as catalyst was performed (Table 1, entries 9–22). In first place, the amount of TBAI was studied (Table 1, entries 6 and 9–11) determining that the reaction undergoes with an optimum yield when this additive is employed at 5 mol% and, in its absence, diphenylbutadiyne was the only reaction product detected (Table 1, entry 9). It is interesting to note that TBAI is employed as source of I^- anions required for the Pd(0) reoxidation to Pd(II) in combination with O_2 and avoiding Pd(0) aggregation.[69–71] Then, the concentration of phenylacetylene **1**, as well as the equivalents of *N*-methylaniline **2**, were studied (Table 1, entries 6 and 12–15) revealing that the reaction proceeds with the best yields at 0.127 M of phenylacetylene **1** and 1.5 equivalents of the amine **2**. Further studies of the reaction parameters showed that better yields of the propiolamide **3** were obtained at a reaction temperature of

Table 1. Pd-catalyzed oxidative aminocarbonylation of phenylacetylene **1** with *N*-methylaniline **2** and CO/O_2. Initial catalytic studies.

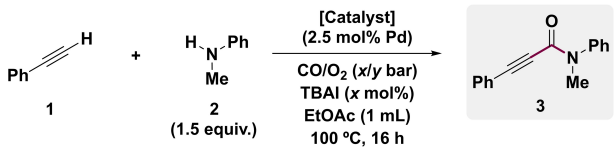

Entry[a]	[Catalyst]-$T_{pyr.}$	TBAI (mol%)	CO/O_2 (bar)	Conv. (%)[b]	**3** (%)[b]
1	$[Pd/La_2O_3]$-500	5	15/5	25	9
2	[Pd/MgO]-500	5	15/5	>99	67
3	$[Pd/CeO_2]$-500	5	15/5	92	52
4	$[Pd/Al_2O_3]$-500	5	15/5	93	56
5	$[Pd/MgAl_2O_4]$-500	5	15/5	37	26
6	**$[Pd/Mg_3Al\text{-}LDH]$-500**	**5**	15/5	**>99**	**88**
7	$[Pd(acac)_2]$	5	15/5	85	45
8	$[Mg_3Al\text{-}LDH]$-500	5	15/5	–	–
9	$[Pd/Mg_3Al\text{-}LDH]$-500	–	15/5	95	–
10	$[Pd/Mg_3Al\text{-}LDH]$-500	2.5	15/5	80	58
11	$[Pd/Mg_3Al\text{-}LDH]$-500	10	15/5	94	76
12[c]	$[Pd/Mg_3Al\text{-}LDH]$-500	5	15/5	80	60
13[d]	$[Pd/Mg_3Al\text{-}LDH]$-500	5	15/5	97	53
14[e]	$[Pd/Mg_3Al\text{-}LDH]$-500	5	15/5	58	41
15[f]	$[Pd/Mg_3Al\text{-}LDH]$-500	5	15/5	75	66
16[g]	$[Pd/Mg_3Al\text{-}LDH]$-500	5	15/5	59	58
17[h]	$[Pd/Mg_3Al\text{-}LDH]$-500	5	15/5	>99	69
18[i]	$[Pd/Mg_3Al\text{-}LDH]$-500	5	15/5	48	40
19[j]	$[Pd/Mg_3Al\text{-}LDH]$-500	5	15/5	94	68
20	$[Pd/Mg_3Al\text{-}LDH]$-500	5	15/2.5	58	45
21	$[Pd/Mg_3Al\text{-}LDH]$-500	5	20/5	80	75
22	$[Pd/Mg_3Al\text{-}LDH]$-500	5	5/1	34	29

[a] Standard reaction conditions: phenylacetylene **1** (14 μL, 0.127 mmol), *N*-methylaniline **2** (21 μL, 0.19 mmol, 1.5 equiv.), [Pd/support]-$T_{pyr.}$ (2.5 mol% Pd, 1.5 wt% Pd in the material, 22.5 mg) where $T_{pyr.}$ = pyrolysis temperature of 500 °C applied under N_2 flow over 3 h and using a heating ramp of 2 °C/min, or $[Pd(acac)_2]$ (2.5 mol% Pd, 0.003 mmol, 1 mg) or $[Mg_3Al\text{-}LDH]$-500 support (22.5 mg), TBAI (tetrabutylammonium iodide) (5 mol%, 0.006 mmol, 2.3 mg), CO/O_2 (15/5 bar), EtOAc (1 mL) at 100 °C during 16 h. [b] Conversion of **1** and yield of **3** were calculated by GC using *n*-dodecane as internal standard. Apart from **3** no other products were detected by GC being the high conversion of **1** attributed to either degradation or polymerization. [c] Run with 0.064 mmol of **1** maintaining 1.5 equiv. of **2**. [d] Run with 0.25 mmol of **1** maintaining 1.5 equiv. of **2**. [e] Run with 1 equiv. of *N*-methylaniline **2**. [f] Run with 2 equiv. of *N*-methylaniline **2**. [g] Run at 80 °C. [h] Run at 120 °C. [i] Run with 1 mol% Pd. [j] Run with 5 mol% Pd.

100 °C and employing a 2.5 mol% of Pd (Table 1, entry 6 and entries 16–19). Several solvents were also evaluated (Table S1, SI), confirming ethyl acetate as the best one. Interestingly, other polar aprotic solvents such as THF, 2-Me-THF and acetonitrile also afforded alkynamide **3** in good yields, in contrast with apolar or polar protic solvents which gave place to poor yields. Finally, several CO/O_2 pressures were explored considering the safe flammability limits[72] (Table 1, entries 6 and 20–22) and it was concluded that the original employed pressures of 15/5 bar were the optimal.

With the aim of further improving the oxidative aminocarbonylation of alkynes, a series of parameters related with the catalyst synthesis were explored and its influence in the catalyst structure and catalytic activity was investigated (Table 2). In first place, the pyrolysis temperature of [Pd/Mg_3Al-LDH] was varied between 150 and 600 °C (Table 2, entries 1–5), concluding that the best yields were achieved at a pyrolysis temperature of 300 °C, reaching high yields of propiolamide **3** even at 80 °C (Table 2, entry 2). Then, several materials pyrolyzed at 300 °C and with different Pd loadings were synthesized and evaluated as catalysts at 60 °C revealing that better yields of **3** were obtained at a Pd loading of 0.75 wt% (Table 2, entry 7), lower than the previously employed of 1.5 wt%. Considering the dramatic influence that pyrolysis temperature can have in LDH structure, materials obtained at pyrolysis temperatures between 150 and 600 °C and with an optimal Pd loading of 0.75 wt%

Table 2. Pd-catalyzed oxidative aminocarbonylation of **1** with **2** and CO/O_2. Influence of the [Pd/Mg_3Al-LDH] pyrolysis temperature applied ($T_{pyr.}$) and Pd (wt %) in the material.

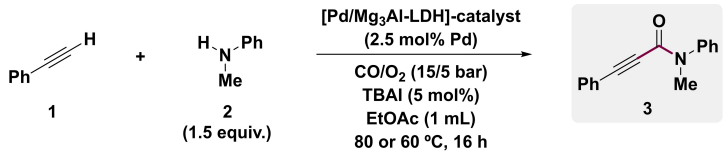

Entry[a]	[Catalyst]-$T_{pyr.}$	Pd (wt%)[b]	T (°C)	Conv. (%)[c]	**3** (%)[c]
1	[Pd/Mg_3Al-LDH]-150	1.5	80	70	69
2	**[Pd/Mg_3Al-LDH]-300**	1.5	80	**94**	**94**
3	[Pd/Mg_3Al-LDH]-400	1.5	80	65	64
4	[Pd/Mg_3Al-LDH]-500	1.5	80	59	58
5	[Pd/Mg_3Al-LDH]-600	1.5	80	61	57
6	[Pd/Mg_3Al-LDH]-300	0.25	60	44	42
7	[Pd/Mg_3Al-LDH]-300	0.75	60	59	58
8	[Pd/Mg_3Al-LDH]-300	1.5	60	44	40
9	[Pd/Mg_3Al-LDH]-300	3	60	38	34
10	[Pd/Mg_3Al-LDH]-150	0.75	60	47	32
11	[Pd/Mg_3Al-LDH]-400	0.75	60	< 10	traces
12	[Pd/Mg_3Al-LDH]-500	0.75	60	< 10	traces
13	[Pd/Mg_3Al-LDH]-600	0.75	60	< 10	traces
14	[Pd/Mg_3Al-LDH]-150	0.75	80	76	73
15	**[Pd/Mg_3Al-LDH]-300**	0.75	80	> **99**	**99**
16	[Pd/Mg_3Al-LDH]-300(A)[d]	0.75	80	72	69
17[e]	[Pd/Mg_3Al-LDH]-300	0.75	80	84	80
18[f]	[Pd/Mg_3Al-LDH]-300	0.75	80	34	33
19[g]	[Pd/Mg_3Al-LDH]-300	0.75	80	60	52
20[h]	[Pd/Mg_3Al-LDH]-300 (1st reuse)	0.75	80	> 99	96
21[h]	[Pd/Mg_3Al-LDH]-300 (2nd reuse)	0.75	80	93	87
22[h]	[Pd/Mg_3Al-LDH]-300 (3rd reuse)	0.75	80	88	80
23[i]	[Pd/C]-commercial	10	80	99	44

[a] Standard reaction conditions: phenylacetylene **1** (14 μL, 0.127 mmol), *N*-methylaniline **2** (21 μL, 0.19 mmol, 1.5 equiv.), [Pd/Mg_3Al-LDH]-$T_{pyr.}$ (2.5 mol% Pd, 0.25 to 3 wt% Pd in the material) where $T_{pyr.}$ = pyrolysis temperature applied under N_2 flow over 3 h and using a heating ramp of 2 °C/min, TBAI (5 mol%, 0.006 mmol, 2.3 mg), CO/O_2 (15/5 bar), EtOAc (1 mL) at 60 or 80 °C during 16 h. [b] Pd (wt%) content in the material measured by ICP-AES. [c] Conversion of **1** and yield of **3** were calculated by GC using *n*-dodecane as internal standard. [d] [Pd/Mg_3Al-LDH]-300(A) corresponds to a version of the material prepared performing metal impregnation onto a previous pyrolized [Mg_3Al-LDH] support (at 300 °C, N_2 flow, 3 h, 2 °C/min) and then pyrolized again under the same conditions. [e] Run with 1.5 mol% Pd. [f] Run during 4 h. [g] Run with CO/O_2 (5/1 bar). [h] Consecutive reuses of the catalytic material performed at standard reaction conditions scaled up to 1.27 mmol of phenylacetylene **1** (see more details in SI), using a freshly pyrolized material (at 300 °C, N_2 flow, 3 h, 2 °C/min) before each new reaction cycle. [i] Pd-material employed by Bhanage in ref. [47] was used under our optimized conditions. Diphenylbutadiyne was the other product detected in this case.

were obtained and tested as catalysts at 60 °C (Table 2, entries 7 and 10–13). At those milder conditions, the only materials that afforded propiolamide **3** in moderate yields of 32 and 58% were the ones pyrolyzed at 150 and 300 °C, respectively (Table 2, entries 7 and 10). To our delight, when the reaction was performed at 80 °C an excellent yield of **3** was obtained employing [Pd/Mg_3Al-LDH]-300 (with a 0.75 wt% Pd) as catalyst (99%, Table 2, entry 15). The synthesis of the optimal [Pd/Mg_3Al-LDH]-300 material was also explored performing the Pd impregnation onto a previously pyrolized [Mg_3Al-LDH]-300 support, affording [Pd/Mg_3Al-LDH]-300(A). However, when [Pd/Mg_3Al-LDH]-300(A) was evaluated as catalyst in the oxidative aminocarbonylation of **1** with **2** in the presence of CO/O_2, lower yields of **3** were obtained than with the previously employed [Pd/Mg_3Al-LDH]-300 catalyst (Table 2, entries 16 and 15). To further explore the influence of the matrix properties in the catalytic activity, several [Pd/Mg_xAl-LDH]-300 materials containing different Mg/Al molar ratios were synthetized[68] and evaluated as catalysts in the studied reaction at 60 °C (Figure S1, SI). Even though all the studied [Pd/Mg_xAl-LDH]-300 materials gave place to the desired propiolamide **3**, [Pd/Mg_3Al-LDH]-300 was the most active of the series. In addition, the catalytic activity of the commercially available [Pd/C] previously employed by Bhanage *et al*[47] in the aminocarbonylation of alkynes with aliphatic amines was compared in our studied reaction at the optimized conditions and showed to be a much less active material (Table 2, entry 23).

Once the synthetic parameters of the optimal catalyst had been determined, we became interested in exploring its catalytic activity at milder conditions such as lower Pd mol%, shorter reaction times and lower CO/O_2 pressures (Table 2, entries 17–19). These studies revealed that the reaction still gave good yields of propiolamide **3** at 1.5 mol% of Pd (80%, Table 2, entry 17), whereas shorter reaction times and milder pressures afforded only moderate yields of **3** (33–52%, Table 2, entries 18 and 19). Moreover, the use of alternative co-oxidants to TBAI was also explored employing optimized [Pd/Mg_3Al-LDH]-300 as catalyst (Table S2, SI). Among all the additives tested, only TBAB afforded **3** in moderate yields and all the other iodide salts or AgOAc only gave traces of the alkynamide of interest **3**, affording mainly the alkyne homocoupling product.

To better understand our active catalytic system, a detailed characterization of the optimal catalyst, [Pd/Mg_3Al-LDH]-300, and some of their structural variations was done. In this sense, it is relevant to consider our initial hypothesis by which designing a material with the optimal acid-base properties can mean a large difference in this kind of oxidative couplings with poorly nucleophilic aromatic amines. Obviously, owing the dramatic effect that pyrolysis temperature of the material has in the catalytic activity, we were very interested in elucidating the structural differences between the materials pyrolyzed at different temperatures. To this end, we characterized [Pd/Mg_3Al-LDH] materials with a Pd loading of 0.75 wt% and pyrolyzed at different temperatures by XRPD, thermogravimetric analysis (TGA), ^{27}Al MAS NMR, CO_2 thermoprogrammed desorption (CO_2-TPD) and BET surface area (Figure 1, Table S4, Figure S18 and Table S7). Interestingly, XRD patterns of the [Pd/Mg_3Al-LDH] materials pyrolyzed at different temperatures showed important differences between them (Figure 1, A). In the case of [Pd/Mg_3Al-LDH] and [Pd/Mg_3Al-LDH]-150, the characteristic (003), (006), (012), (015), (018), (110) and (113) reflections at 2θ 11.7, 23.5, 35.0, 39.5, 47.0, 60.8 and 62.2° appeared in the corresponding diffractograms and were assigned to a rhombohedral (3R) LDH structure (JCPDS-541030).[61,73–75] Moreover, no differences were observed between the XRD patterns of these materials and the one corresponding to [Mg_3Al-LDH] (Figure S8), which indicates the high crystallinity and order of [Pd/Mg_3Al-LDH] and [Pd/Mg_3Al-LDH]-150. In addition, the presence of large Pd nanoparticles in their structure was totally discarded. On the other hand, in the corresponding [Pd/Mg_3Al-LDH] materials pyrolyzed at 400, 500 and 600 °C the characteristic patterns (200) and (220) of a MgO-periclase phase (2θ 43.6 and 63.1°) appeared together with a weak LDH phase (Figure 1, A). By contrast, the patterns of Al_2O_3 were not detected, suggesting the formation of an amorphous phase. Thus, the formation of a mixed oxide $MgAlO_x$ is proposed for these materials pyrolized at $\geq$400 °C. At these temperatures, it is possible the collapse of the LDH structure by partial dehydroxylation of the brucite-like sheets followed by hydroxyl condensation.[61,73,76–77] In this point, it is interesting to note that in [Pd/Mg_3Al-LDH]-600 the characteristic (111), (200), (220) and (311) reflections attributed to Pd(0) nanoparticles were identified (JCPDS 00-046-1043), although in very low intensity, indicating the presence of Pd(0) nanoparticles with sizes around 4–5 nm in this material. Interestingly, the most active material, [Pd/Mg_3Al-LDH]-300, showed a different XRD pattern with respect to both LDH and MMO materials, whereas with strong similarities with the former ones. More specifically, XRD pattern of [Pd/Mg_3Al-LDH]-300 (Figure 1, A) clearly shows (003) and (110) characteristic reflections of LDH, although in a much broader fashion than in [Mg_3Al-LDH], [Pd/Mg_3Al-LDH] and [Pd/Mg_3Al-LDH]-150, indicating a higher degree of disorder in this case. In fact, the corresponding Scherrer dimensions of D_{003} and D_{110} are dramatically reduced to 2.59 nm and 8.03 nm respectively, in comparison with the values obtained for [Mg_3Al-LDH], [Pd/Mg_3Al-LDH] and [Pd/Mg_3Al-LDH]-150 of 30.95–33.91 nm and 24.49–29.06 nm.[78] It is also relevant to consider that (006), (012), (015), (018) and (113) typical reflections of LDH are not observed in [Pd/Mg_3Al-LDH]-300, whereas a new line at 2θ 36.5° appears. This kind of XRD pattern in LDH materials pyrolized or calcined at relatively low temperatures has been previously studied by several research groups and it has been assigned to dehydrated LDH materials (dh-LDH), an intermediate phase between a LDH and a MMO.[61,73,76,78] A careful analysis of (003) reflection 2θ value of [Pd/Mg_3Al-LDH]-300 in comparison with the ones found for [Mg_3Al-LDH] and [Mg_3Al-LDH]-300 shows a shift to higher angles in the case of the materials pyrolized at 300 °C, which means a decrease in basal spacing *d* as well as in the lattice parameter *c* (Table S4). This effect is explained by the removal of the interlayer water present in LDH and, hence, the formation of a dehydrated LDH material. However, here it is important to remark that in our case the dehydration is only partial, as the observed decrease in basal spacing is clearly

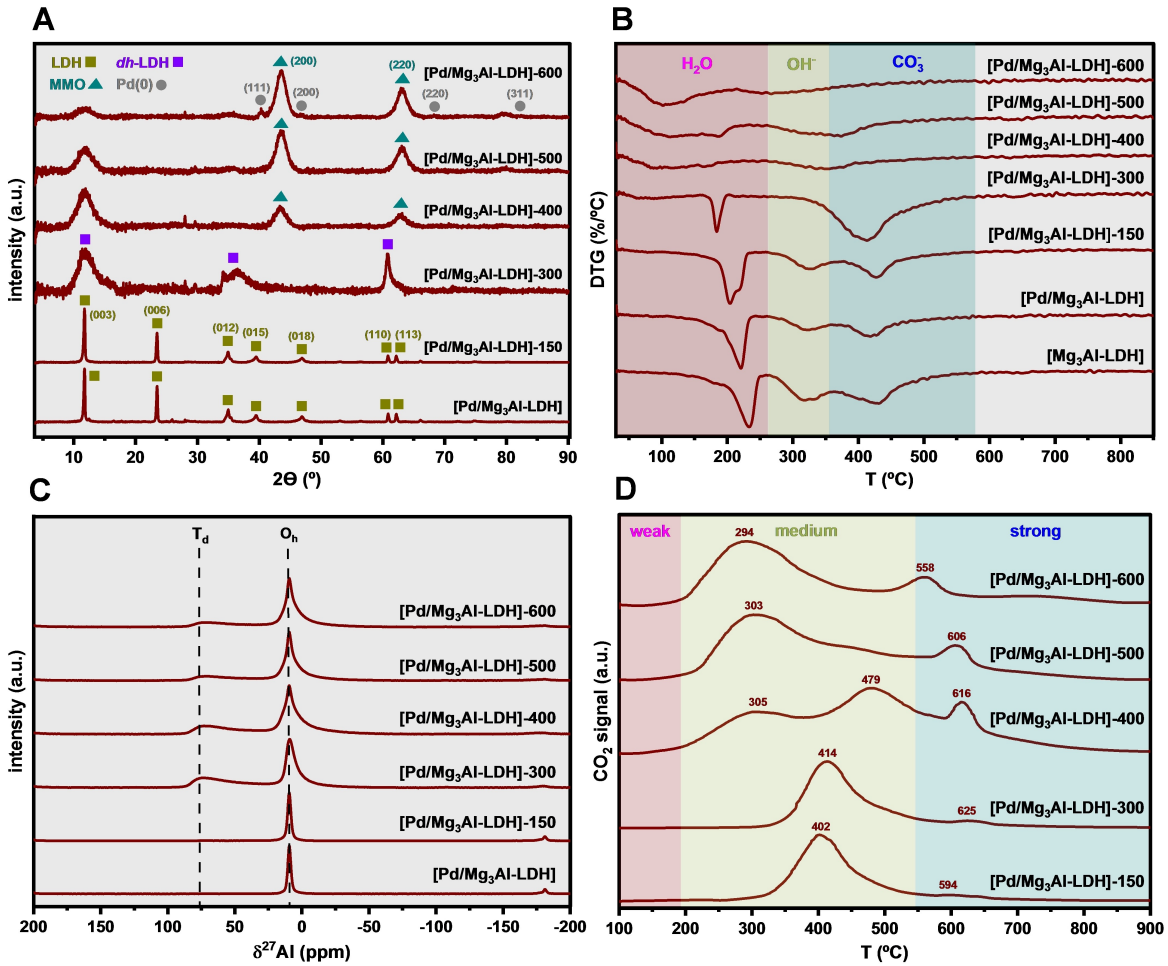

Figure 1. (A) XRPD patterns, (B) DTG profiles, (C) ^{27}Al MAS NMR spectra and (D) CO_2-TPD analysis of selected [Pd/Mg_3Al-LDH] materials (with a 0.75 wt% Pd) and [Mg_3Al-LDH] support. JCPDS 00-046-1043 comprises the reference diffractogram used for the assignment of the metallic Pd phases (111), (200), (220) and (311), JCPDS-541030 for LDH phases (003), (006), (012), (015), (018), (110) and (113), and JCPDS 71-1176 for MMO phases (200) and (220).

minor than the observed in other reported dh-LDH (Table S4).[61,76,78] Moreover, (110) reflection 2θ values at [Pd/Mg_3Al-LDH]-300 XRD did not change with respect to [Mg_3Al-LDH], [Pd/Mg_3Al-LDH] and [Pd/Mg_3Al-LDH]-150 (Table S4), confirming that *a* cell parameter, related with cation-cation distance, was not altered at 300 °C, and suggesting that the layered structure was maintained at this temperature. It is also important to remark that XRD of [Pd/Mg_3Al-LDH]-300 did not show any peak assigned to the presence of Pd nanoparticles. Furthermore, the XRD patterns of [Pd/Mg_3Al-LDH] materials pyrolized at different temperatures (150–600 °C) and with a higher Pd charge of 1.5 wt%, showed an analogous behavior to the one described for 0.75 wt% Pd charged materials (Figure S9 vs Figure 1, A). In addition, other materials pyrolized at 300 °C such as [Pd/Mg_3Al-LDH]-300 with different Pd loadings (0.25–3 wt% Pd) (Figure S10), [Pd/Mg_3Al-LDH]-300(A) (Figure S12) or [Pd/Mg_xAl-LDH]-300 (Figures S14–16) showed XRD patterns similar to the ones observed for [Pd/Mg_3Al-LDH]-300. It is also relevant to note that [Pd/Mg_3Al-LDH]-300 after 10 days of its pyrolysis showed the same XRD pattern (Figure S11), which indicates the stability of the partially dehydrated LDH structure.

Thermogravimetric analysis further confirmed the partially dehydrated LDH structure of the optimal catalyst [Pd/Mg_3Al-LDH]-300 (Figure 1, B). Thermal decomposition of LDH materials has been intensively studied in the literature and several authors have reported that, upon thermal treatment, there is a first loss of interlayer water (50–225 °C) to give a dh-LDH stable intermediate phase, followed by a dehydroxylation/decarbonation coupled process to give a LDH-derived mixed oxide at more than 350 °C.[61,79–80] Despite being a coupled process, it has been demonstrated that dehydroxylation starts in first place, although in a low degree, at temperatures higher than 200 °C.[61] TGA and DTG of [Pd/Mg_3Al-LDH]-300 (Figure 1, B and Figure S18) show that our optimal catalyst still presents a characteristic interlayer water loss at a temperature lower than 250 °C, although less intense than for [Pd/Mg_3Al-LDH] and [Pd/Mg_3Al-LDH]-150, which would confirm its partial dehydration. Interestingly, [Pd/Mg_3Al-LDH]-300 shows an important mass loss between 320 and 530 °C that can be assigned to the simultaneous loss of hydroxyl and carbonate groups. In contrast, [Mg_3Al-LDH], [Pd/Mg_3Al-LDH] and [Pd/Mg_3Al-LDH]-150 materials present, as well as a larger loss of interlayer water at a temperature lower than 250 °C, the hydroxyl and carbonate

groups loss in two phases, one at $<350\,^{\circ}C$ and another at $<450\,^{\circ}C$ (Figure 1, B). This evidence further supports the different LDH structure of [Pd/Mg_3Al-LDH]-300 and suggests a partial loss of hydroxyl groups in this material. In addition, thermogravimetric study of [Pd/Mg_xAl-LDH]-300 materials was also performed (Figure S20) and, for materials with a Mg/Al ratio different to 3, the loss of interlayer water was observed at lower temperatures and with less intensity. Hence, it is possible that in the optimum [Pd/Mg_3Al-LDH]-300 catalyst, the interlayer water is interacting with higher strength. DTG profiles of materials pyrolized at $\geq 400\,^{\circ}C$ confirm their MMO structure (Figure 1, B).

Moreover, the partial dehydroxylation of [Pd/Mg_3Al-LDH]-300 was confirmed by ^{27}Al MAS NMR. In fact, in Figure 1, C can be observed that, while [Pd/Mg_3Al-LDH] and [Pd/Mg_3Al-LDH]-150 present only a sharp signal at 10 ppm characteristic of Al centers with octahedral (O_h) symmetry, [Pd/Mg_3Al-LDH]-300 displays also another signal around 75 ppm assigned to tetrahedral geometry (T_d) Al centers.[73,79,81] Both signals in this material present a broad shape suggesting a disorted geometry. Materials pyrolized at 300 °C with a different Mg/Al molar ratio, [Pd/Mg_xAl-LDH]-300 (Figure S22), as well as [Pd/Mg_3Al-LDH] materials pyrolized at temperatures larger than 300 °C (Figure 1, C) also displayed similar ^{27}Al MAS NMR spectra with characteristic signals of octahedral (O_h) and tetrahedral geometry (T_d) Al centers. To further characterize [Pd/Mg_3Al-LDH] materials pyrolized at different temperatures, they were analyzed by CO_2-TPD (Figure 1, D and Table S8). In the case of [Pd/Mg_3Al-LDH]-150 and [Pd/Mg_3Al-LDH]-300, a single signal centered at 402–414 °C was detected, coinciding with the temperature of interlayer carbonate decomposition. Hence, for these materials with LDH or partially dehydrated LDH structure it was not possible to quantify their basic properties through this method.[73] By contrast, [Pd/Mg_3Al-LDH]-400, [Pd/Mg_3Al-LDH]-500 and [Pd/Mg_3Al-LDH]-600 with MMO structure show CO_2 desorptions at a maximum temperature between 294–479 °C, associated with moderate basic sites, and 558–625 °C, corresponding with strong basic sites. In addition, the density of their basic sites was quantified (Table S8) and it resulted to be between 11.2–36.4 μmol CO_2/g.[73] Then, BET surface areas of the [Pd/Mg_3Al-LDH] materials pyrolized at different temperatures were quantified by nitrogen adsorption-desorption isotherms (Table S7). An increase of the area was observed with the increase in the pyrolysis temperature, reaching the highest values (125.0–256.4 m^2/g) for the materials with MMO structure.[73] In the case of our optimal catalyst, [Pd/Mg_3Al-LDH]-300, an area of 12.3 m^2/g was measured, similar to the ones of LDH materials.

To complete the characterization of [Pd/Mg_3Al-LDH]-300, it was examined by high-angle annular dark-field-high-resolution scanning transmission electron microscopy (HAADF-HRSTEM), high resolution transmission electron microscopy (HR-TEM) and energy dispersive X-ray (EDX) elemental analysis (Figure 2 and Figure S26). Average Pd nanoparticles of 2.8 nm were measured and its homogeneous dispersion over the partially dehydrated LDH support was confirmed through EDX mapping.

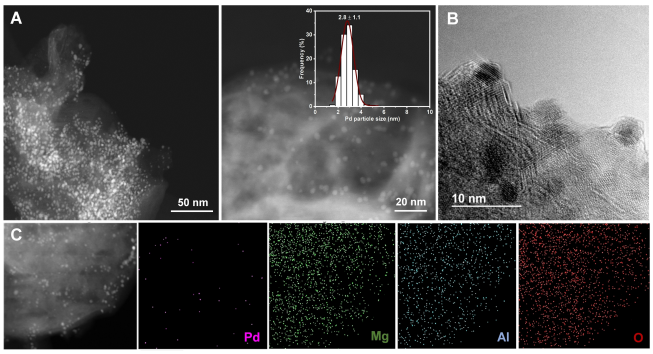

Figure 2. (A) HAADF-HRSTEM images and Pd particle size distribution, (B) HRTEM images and (C) EDX elemental mapping analysis of Pd, Mg, Al and O for [Pd/Mg_3Al-LDH]-300 material.

At this point, we became interested in investigating the kinetic features of our studied catalytic system. With this aim, the yield time kinetic profile of the aminocarbonylation of phenylacetylene **1** with *N*-methylaniline **2** at the optimized conditions and catalyzed by [Pd/Mg_3Al-LDH]-300 was investigated (Figure 3, A and B, Figure S2). In this experiment, an initial rate of 5.5 %/h for product **3** formation was measured, and an induction period of 15 minutes was detected. The presence of this induction period suggested a change in the Pd centers nature under our reaction conditions. Hence, we synthesized, characterized by XPS and catalytically evaluated a series of materials in which [Pd/Mg_3Al-LDH] was subjected to a thermal treatment under different atmosphere conditions (Figure 3, Figures S3–S5). Thus, [Pd/Mg_3Al-LDH]-300(B) was obtained through calcination under air at 300 °C, while [Pd/Mg_3Al-LDH]-300(C) was synthesized after reduction with H_2 at the same temperature. In addition, [Pd/Mg_3Al-LDH]-300(D) was obtained after a first pyrolysis under N_2 at 300 °C followed by a reduction with H_2 at 200 °C. To our delight, [Pd/Mg_3Al-LDH]-300(D) improved the obtained results with our up to now optimal catalyst, [Pd/Mg_3Al-LDH]-300, as it afforded quantitative yields of alkynamide **3** with a 10.4 %/h of initial rate and avoiding the induction period (Figure 3, A and B, Figure S5). Interestingly, [Pd/Mg_3Al-LDH]-300(C), subjected to a hydrogenating treatment at 300 °C, also avoided the induction period, but afforded alkynamide **3** in lower yield and initial rate (77 % and 5.9 %/h) than the material first pyrolyzed at 300 °C and then hydrogenated at 200 °C (Figure 3, A and B, Figure S4). By contrast, [Pd/Mg_3Al-LDH]-300(B), obtained by calcination, gave a low yield of **3** (35 %), a lower initial rate (3.6 %/h) and presented a longer induction period of 30 minutes (Figure 3, A and B, Figure S3). Thus, both materials with a pyrolysis treatment, [Pd/Mg_3Al-LDH]-300 and [Pd/Mg_3Al-LDH]-300(D), gave place to the best yields of product **3**, while only the hydrogenated materials avoided induction period.

With the aim of elucidating which kind of Pd species constitute these materials and being able to stablish a relationship between their nature and their catalytic activity, the four materials were analyzed by X-ray photoelectron spectroscopic (XPS) technique (Figure 3, C–F). The Pd 3d spectrum of [Pd/Mg_3Al-LDH]-300 could be deconvoluted in four peaks corre-

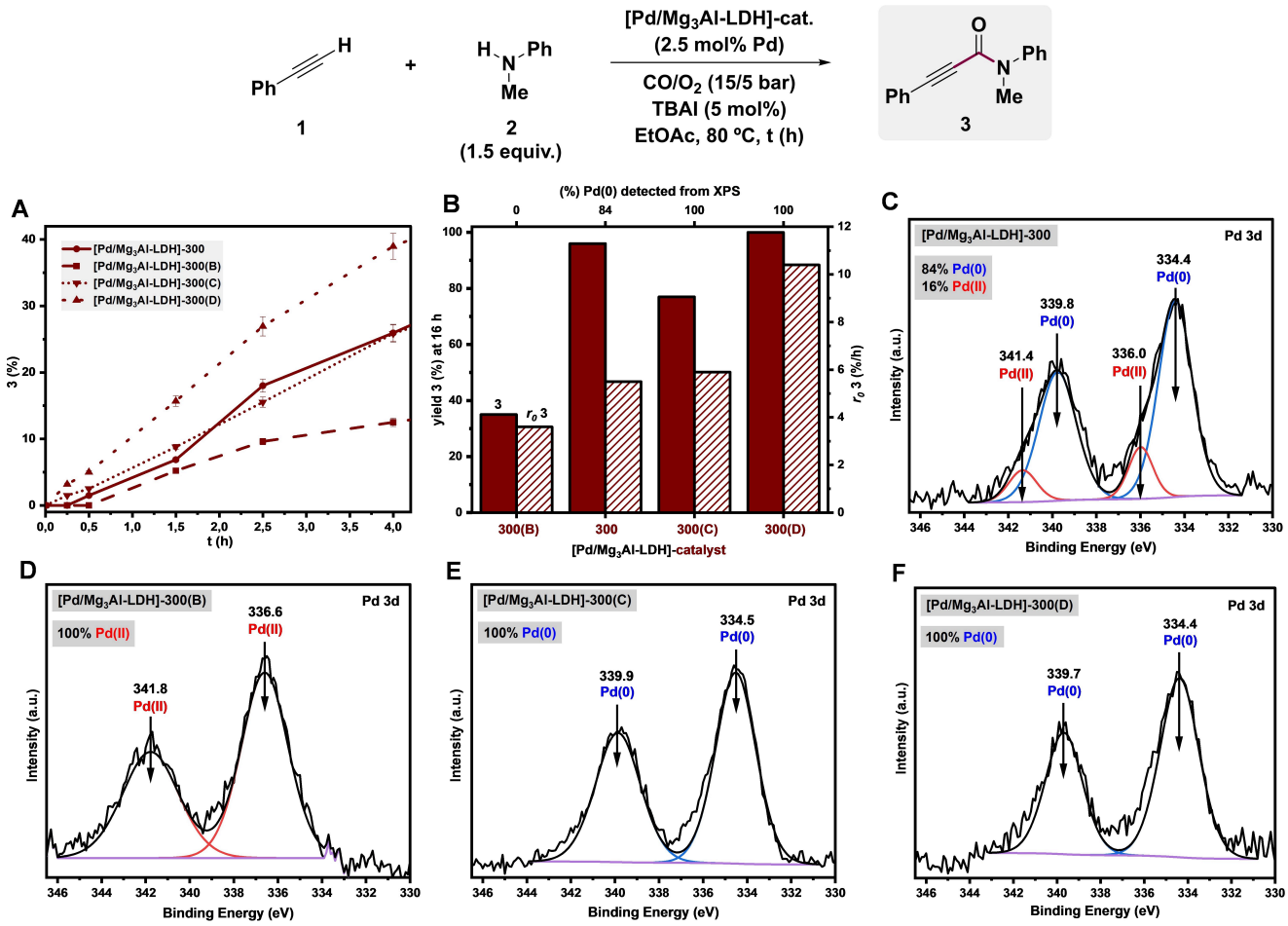

Figure 3. (A) Yield/time profile for the oxidative aminocarbonylation of **1** with **2** and CO/O_2 in the presence of different [Pd/Mg_3Al-LDH] materials. (B) Yield (at 16 h) and initial rate of formation of product **3** *vs* [%Pd(0)] detected by XPS analysis for different [Pd/Mg_3Al-LDH] materials. Initial rate (r_0) is the slope of the linear equation: [**3** (%) = r_0×t (h)] defined at initial reaction times and expressed as [**3** (%/h)] and without considering the points corresponding to the induction period. (C–F) Pd 3d XPS spectra of [Pd/Mg_3Al-LDH]-300, [Pd/Mg_3Al-LDH]-300(B), [Pd/Mg_3Al-LDH]-300(C) and [Pd/Mg_3Al-LDH]-300(D) materials. [Pd/Mg_3Al-LDH]-300: pyrolized at 300 °C under N_2 flow; [Pd/Mg_3Al-LDH]-300(B): calcined at 300 °C under air flow; [Pd/Mg_3Al-LDH]-300(C): reduced at 300 °C under H_2 flow. [Pd/Mg_3Al-LDH]-300(D): pyrolized at 300 °C under N_2 flow and then reduced at 200 °C under H_2 flow.

sponding to two doublets: one at 334.4 eV ($3d_{5/2}$) and 339.8 ($3d_{3/2}$) corresponding to Pd(0) and another at 336.0 eV ($3d_{5/2}$) and 341.4 eV ($3d_{3/2}$) belonging to Pd(II). Considering a depth of measure in XPS around 6–8 nm, it could be quantified the percentage of Pd(0) in 84%. By contrast, Pd 3d XPS spectrum of [Pd/Mg_3Al-LDH]-300(B) only showed a doublet at 336.6 eV ($3d_{5/2}$) and 341.8 eV ($3d_{3/2}$) assigned to Pd(II), while the two materials subjected to an hydrogenating treatment, [Pd/Mg_3Al-LDH]-300(C) and [Pd/Mg_3Al-LDH]-300(D), displayed a doublet at 334.4–335.5 eV ($3d_{5/2}$) and 339.7–339.9 eV ($3d_{3/2}$) belonging to Pd(0). Therefore, it appears that the two materials constituted by only Pd(0) species, [Pd/Mg_3Al-LDH]-300(C) and [Pd/Mg_3Al-LDH]-300(D), are the only ones not showing an induction period. Considering the oxidative nature of this reaction, this observation resulted in principle quite surprising. To further understand the nature of these materials, their Mg 1s XPS spectra was analyzed in comparison with the corresponding spectrum of [Mg_3Al-LDH]-300 (Figure S25). For all the materials, an upshifting of the binding energy between 1 and 1.6 eV was observed with respect to the support, which can be interpreted as a decrease in electron density of Mg^{2+} species due to the electron transfer from LDH Mg^{2+}-OH group to Pd.[78] Moreover, additional characterization was performed for [Pd/Mg_3Al-LDH]-300(B), [Pd/Mg_3Al-LDH]-300(C) and [Pd/Mg_3Al-LDH]-300(D) by XRD (Figure S17), and ^{27}Al NMR MAS (Figure S23), which confirmed their partially dehydrated LDH structure.

Despite the similar nature of Pd in both hydrogenated materials, [Pd/Mg_3Al-LDH]-300(C) and [Pd/Mg_3Al-LDH]-300(D), they showed important differences regarding their catalytic activity (Figure 3). To better understand this phenomenon, we considered the possible reduction of the matrix under their synthesis and studied [Mg_3Al-LDH] temperature programmed reduction (Figure S28). Thus, in the TPR profile of this LDH material two positive peaks at maximum temperatures of 404 and 579 °C were observed, associated with the reduction of this material, together with a negative peak at 492 °C that can be explained by a H_2 release. It is important to note that under this thermal treatment MMO phases should be generated and it has been reported in the literature the MgO capacity to adsorb and release hydrogen.[82] Considering that the first H_2 adsorption

starts at temperatures near 300 °C, it is reasonable to propose that the lower catalytic activity of [Pd/Mg_3Al-LDH]-300(C) could be influenced by the different nature of the support in this material reduced at 300 °C.

To gain further evidences that assist us in the understanding of the reaction mechanism and its relationship with the material structure, we investigated [Pd/Mg_3Al-LDH]-300 structure after reaction by XRPD (Figure S13), ^{27}Al MAS NMR (Figure S21), HAADF-HRSTEM (Figure S27) and XPS (Figure S24). XRD and ^{27}Al MAS NMR did not show any significant change with respect to the fresh material, confirming that the partially dehydrated LDH structure was maintained after reaction and no large Pd nanoparticles appeared. Moreover, the absence of large Pd nanoparticles was confirmed by HAADF-HRSTEM that showed a good dispersion of Pd species with an average size of 3.3 nm. XPS study of the used [Pd/Mg_3Al-LDH]-300 material displayed a Pd 3d spectrum with two doublets assigned to Pd(II) and Pd(0), with very similar binding energy values to the ones found in the fresh material. In addition, a similar proportion of Pd(0) and Pd(II) could be quantified, 76% of Pd(0) and 24% of Pd(II). Mg 1s spectrum also showed a signal at very similar binding energy to the one found for the fresh [Pd/Mg_3Al-LDH]-300. Interestingly, a doublet in the I 3d area was detected at 618.5 eV ($3d_{5/2}$) and 630.0 eV ($3d_{3/2}$). It has been described in the literature that I $3d_{5/2}$ BE for I atomically located on metal surfaces is expected between 618.5 and 619.7 eV.[83] Hence, our results suggest that iodide from TBAI could be interacting with Pd nanoparticles forming [PdI_2] species onto the support surface.[84]

Considering all these results, and discarding a radical type pathway (Table S3), we have proposed a mechanism (Figure 4) in which the main active species are [PdI_2] centers located in the surface of the matrix support. In the context of an oxidative process, the presence of an induction period only for the materials containing Pd(II) species in their structure could be explained if a first fast oxidation of iodide from TBAI occurs. Thus, in the presence of I_2, the formation of the [PdI_2] centers would be more efficient through a redox process with Pd(0) centers. In fact, this was confirmed performing the reaction with [Pd/Mg_3Al-LDH]-300(D) as catalyst and employing I_2 an additive in 2.5 mol% instead of TBAI. Under these reaction conditions, the corresponding propiolamide **3** was obtained with a 78% yield. This would explain the better catalytic activity of [Pd/Mg_3Al-LDH]-300(D), as well as the absence of an induction period for the two hydrogenated materials. By contrast, [Pd/Mg_3Al-LDH]-300(B), with only Pd(II) species, would have more difficulties in forming [PdI_2] centers in the presence of large amounts of I_2, which would explain its worse catalytic activity and long induction period. On the other hand, the presence of an induction period of 15 minutes in the case of [Pd/Mg_3Al-LDH]-300 with a 16% of Pd(II), would be explained if this oxidized Pd species are more abundant in the surface of the Pd nanoparticles (Figure 4). Once [PdI_2] centers are formed onto the surface matrix support (intermediate **II**), we propose that the mechanism undergoes through the first activation of the corresponding amine mediated by LDH basic centers (intermediate **III**), followed by its Pd coordination and CO insertion to give intermediate **IV**. Then, the alkyne activation mediated by LDH basic centers and its coordination to Pd centers should occur to form intermediate **VI**. This intermediate could undergo reductive elimination to finally afford the alkynamide and **VII** containing Pd(0) centers, which should get reactivated through its oxidation in the presence of O_2 and iodides.

The heterogeneous nature of the most active catalysts, [Pd/Mg_3Al-LDH]-300 and [Pd/Mg_3Al-LDH]-300(D), was verified by a filtration test (see SI, section 6.1, Figures S6 and S7). Moreover, the reaction mixtures after these experiments were analyzed by inductively coupled plasma (ICP) indicating only a 3% of Pd leached (see SI, section 6.2). ICP measurements were also performed in the catalysts after usual reaction conditions confirming a good stability in the Pd content of the materials after their use (0.72 wt% *vs* 0.75 wt% in the fresh materials). Hence, the reusability of the catalytic system was studied with [Pd/Mg_3Al-LDH]-300, for practical reasons, and using a freshly pyrolized material after each use to ensure organic material elimination. Gratifyingly, the catalyst resulted reusable for three catalytic cycles (Table 2, entries 20–22).

Having established the remarkable catalytic performance of [Pd/Mg_3Al-LDH]-300(D) for promoting the aminocarbonylation of **1** with **2** in the presence of CO/O_2, as well as its robustness, we became interested in evaluating its range of synthetic applicability in the aminocarbonylation of a variety of terminal alkynes in combination with a broad diversity of aromatic and aliphatic amines (Scheme 2 and 3). Initially, *N*-methylaniline **2** was reacted under the optimized conditions (2.5 mol% Pd catalyst with a 0.75 wt% Pd in the material, 5 mol% TBAI, 15 bar CO, 5 bar O_2, 80 °C, 16 h and EtOAc as solvent) with a wide variety of aromatic alkynes (Scheme 2). In specific cases and to ensure a total conversion of the alkyne and/or improving final propiolamide yield, reaction conditions implying larger CO/O_2 pressures (20/5 bar) and higher reaction temperature (120 °C) were applied. To our delight, apart from *N*-methyl-*N*,3-diphenylpropiolamide **3** isolated in 90% yield, several substituted propiolamides, **4**–**15**, obtained from *orto*-, *meta*-, and *para*-substituted phenylacetylenes could be isolated in moderate to excellent yields (58–91%). It is important to note that our protocol tolerated either phenylacetylenes bearing electron-donating groups (EDG) such as methyl, methoxy or dimethylamino, as well as electron-withdrawing groups (EWG) as trifluoromethyl, nitro, chloride or methylcarboxylate. In addition, 1-ethynylnaphthalene in combination with **2** also afforded the desired propiolamide product **16** in 69% yield. Relevant heteroaromatic alkynes, containing pyridine and thiophene scaffolds in their structure yielded the desired *N*-methyl-*N*-aryl-3-heteroarylpropiolamides **17**–**19** very efficiently (74–80%). Harsher conditions regarding temperature and pressure were employed with some electron deficient alkynes, such as chlorine, trifluoromethyl or nitro substituted phenylacetylenes, as well as pyridine substituted alkynes. Gratifyingly, our designed [Pd/Mg_3Al-LDH]-300(D) system was also highly effective to perform the aminocarbonylation between *N*-methylaniline **2** and challenging aliphatic terminal alkynes. Thus, a variety of aliphatic alkynes either featuring linear and cyclic chains,

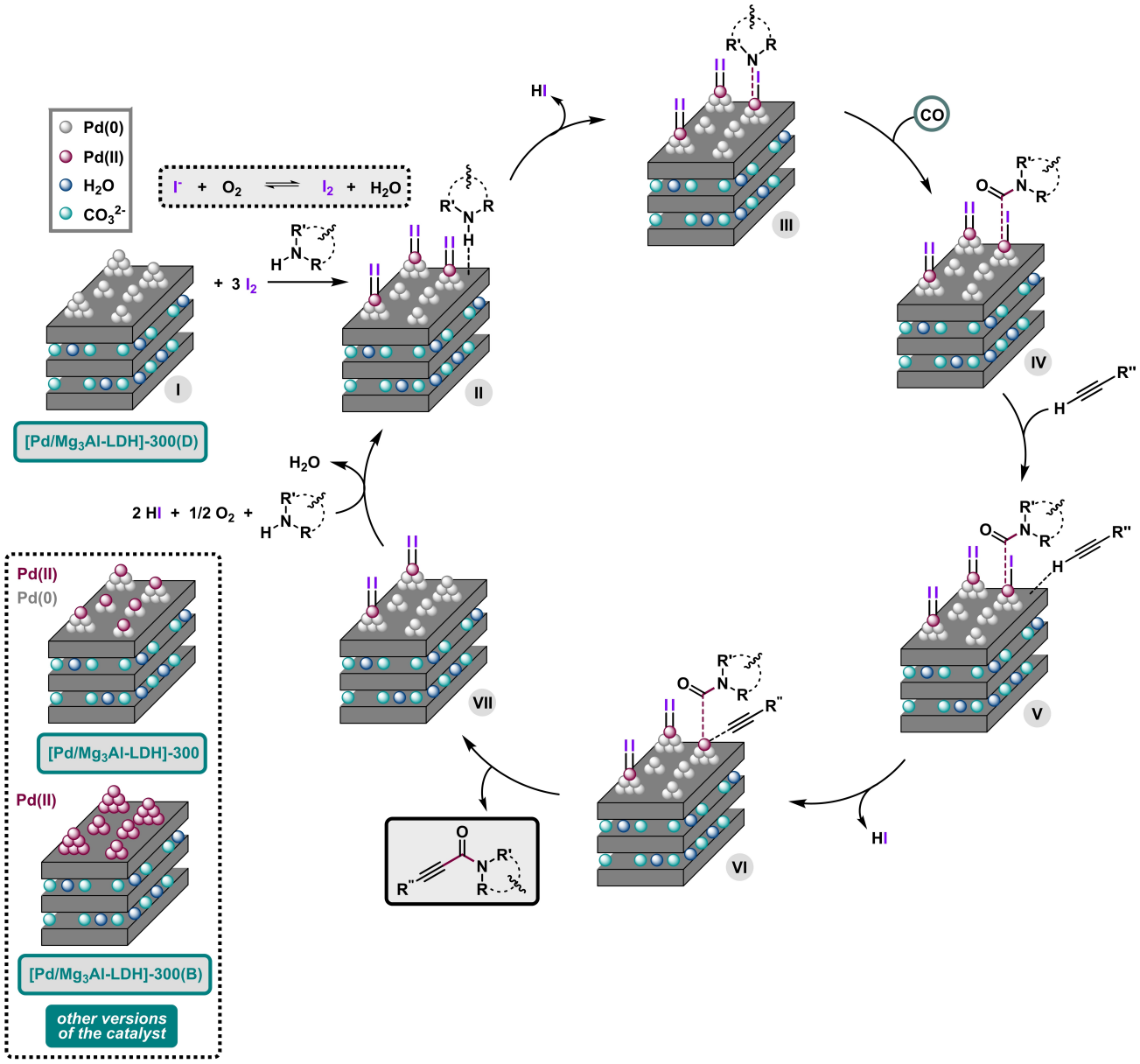

Figure 4. Proposed mechanism for the [Pd/Mg_3Al-LDH]-300(D)-catalyzed oxidative aminocarbonylation of alkynes with amines and CO/O_2 mixture. [Pd/Mg_3Al-LDH]-300 and [Pd/Mg_3Al-LDH]-300(B) schematic representations.

with an internal cyclic alkene and hydroxy or phthalimido groups as substituents were fully tolerated producing the desired *N*-methyl-*N*-phenyl-3-alkyl(substituted)propiolamides **20**–**25** in 58–88% isolated yields.

As commented above, up to date there is no described protocol for performing the oxidative aminocarbonylation of alkynes with aromatic amines due to the low nucleophilicity of these substrates. Considering that our methodology resulted successful employing *N*-methylaniline **2**, the evaluation of a large diversity of aromatic amines, including *N*-heterocycles, was of interest. Scheme 3 showcases this study in which we could prove the large versatility of our catalytic protocol for performing the aminocarbonylation of phenylacetylene **1** with a wide range of *N*-(hetero)aryl-based amines. In general, with few exceptions, for achieving good yields of the corresponding alkynamide target compounds, slightly harsher conditions (120 °C and 20/5 bar of CO/O_2 mixture) were needed. To our delight, [Pd/Mg_3Al-LDH]-300(D) nanocatalyst was highly effective towards the aminocarbonylation of phenylacetylene **1** with several *N*-methyl(substituted) anilines bearing either EDG (methyl, phenyl, methoxy, trifluoromethoxy) or EWG (halogen or nitrile) as substituents in *orto*, *meta*- and *para*-positions and affording propiolamides **26**–**35** in 69–95% isolated yields. In fact, even halogen-disubstituted anilines, yielded the desired propiolamides **36** and **37** in good yields (68–83%). In addition, *N*-methylnaphthalen-1-amine and *N*-methylpyridin-3-amine, as an example of interesting heteroaromatic aniline, were also

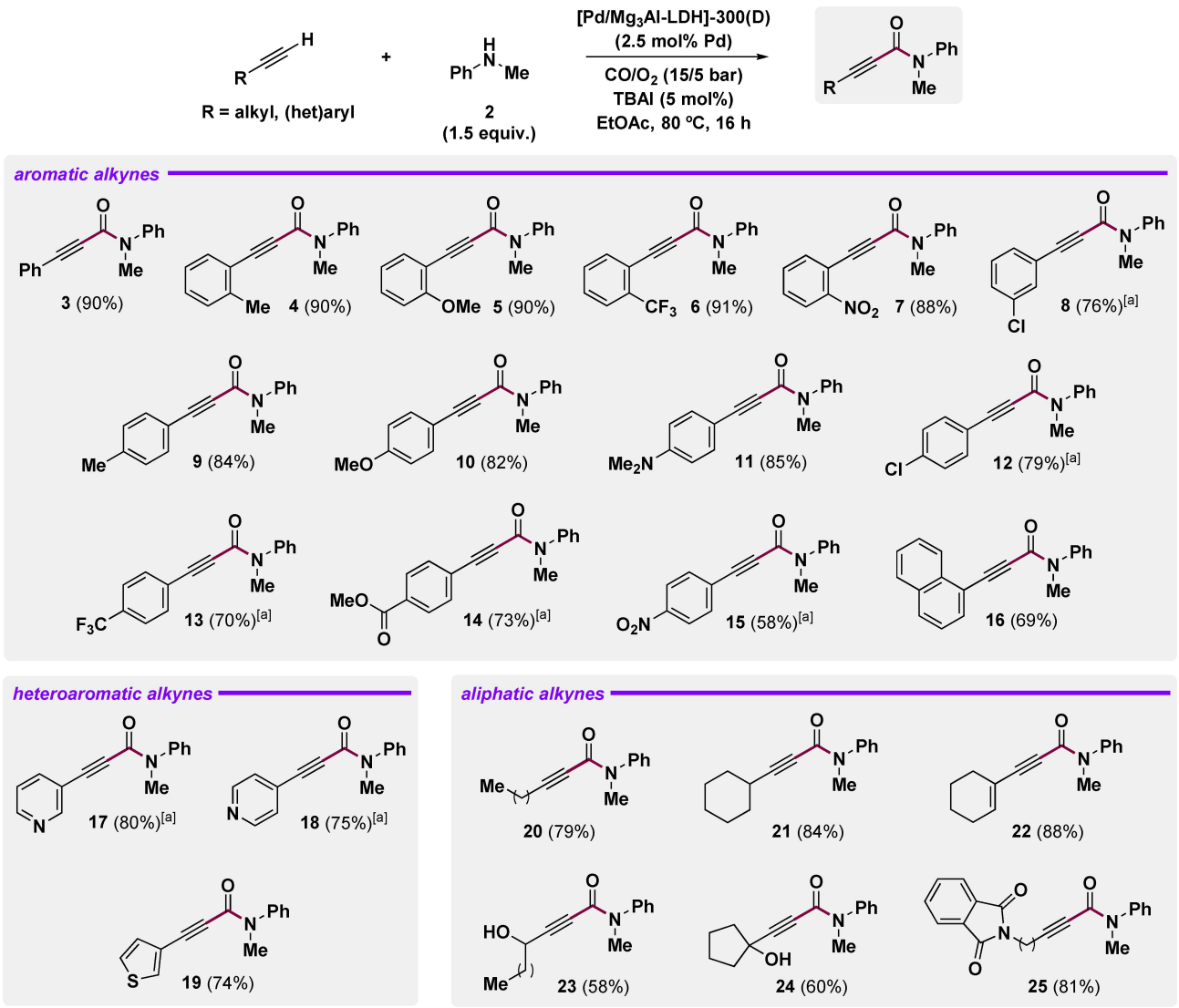

Scheme 2. [Pd/Mg_3Al-LDH]-300(D)-catalyzed oxidative aminocarbonylation of (hetero)aromatic and aliphatic terminal alkynes with *N*-methylaniline **2** and CO/O_2. Standard reaction conditions: alkyne (0.127 mmol), *N*-methylaniline **2** (21 μL, 0.19 mmol, 1.5 equiv.), [Pd/Mg_3Al-LDH]-300(D) (2.5 mol% Pd, 0.75 wt% Pd in the material, 45 mg), TBAI (5 mol%, 0.006 mmol, 2.3 mg), CO/O_2 (15/5 bar), EtOAc (1 mL) at 80 °C during 16 h. Isolated yields after column chromatography on silica are given between parentheses. [a] Run under CO/O_2 (20/5 bar) at 120 °C.

successfully employed and gave place to the target products **38** and **39** in 72 and 60%, respectively.

Furthermore, several *N*-alkylanilines with a variety of primary and sterically hindered secondary alkyl groups, such as *i*-Pr, cyclohexyl and benzyl-, were exposed to the reaction conditions and the corresponding products **40**–**44** were accessed in 69–80% yields after isolation. Interestingly, two highly challenging *N,N*-diarylamines could be converted to the desired *N,N*,3-tris(arylsubstituted)propiolamides **45** and **46** in moderate to good yields after isolation (47 and 87%, respectively). At this point, we were interested in applying our catalytic protocol to the employment of relevant *N*-aryl based heterocycles as amine nucleophiles in the oxidative aminocarbonylation of **1**. Gratifyingly, several *N*-aryl heterocycles including indolines, indols and tetrahydroquinolines bearing several types of chemical substitution such as methyl, bromine, methoxy, fluoro and even nitro groups underwent the desired reaction giving the target *N*-(aryl-based heterocycle)-3-aryl-propiolamides **47**–**56** in good to excellent isolated yields (63–97%). Notably, this is the first example where this kind of *N*-heterocyclic amines have been employed as nucleophiles in this reaction. Finally, our developed Pd nanocatalyst demonstrated a remarkable applicability in the aminocarbonylation of **1** with *N,N'*-dialkylamines or *N*-alkyl based heterocycles as nucleophiles. Given the higher nucleophilicity of aliphatic amines, milder reaction conditions could be employed in these cases (5 bar CO, 1 bar O_2 and 80 °C). By using that conditions, several *N*-alkyl-3-arylpropiolamides **57**–**65** were obtained in excellent isolated yields (79–98%). It is interesting to remark the high chemoselectivity *N*- vs *O*-nucleophile observed in the formation of the propiolamide **59** (79%). Furthermore, propiolamide **63**, a structural derivative of the drug donepezil® used for

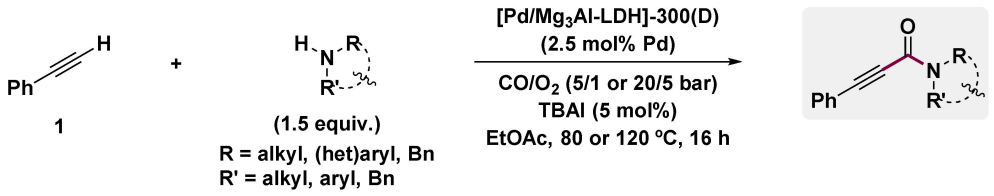

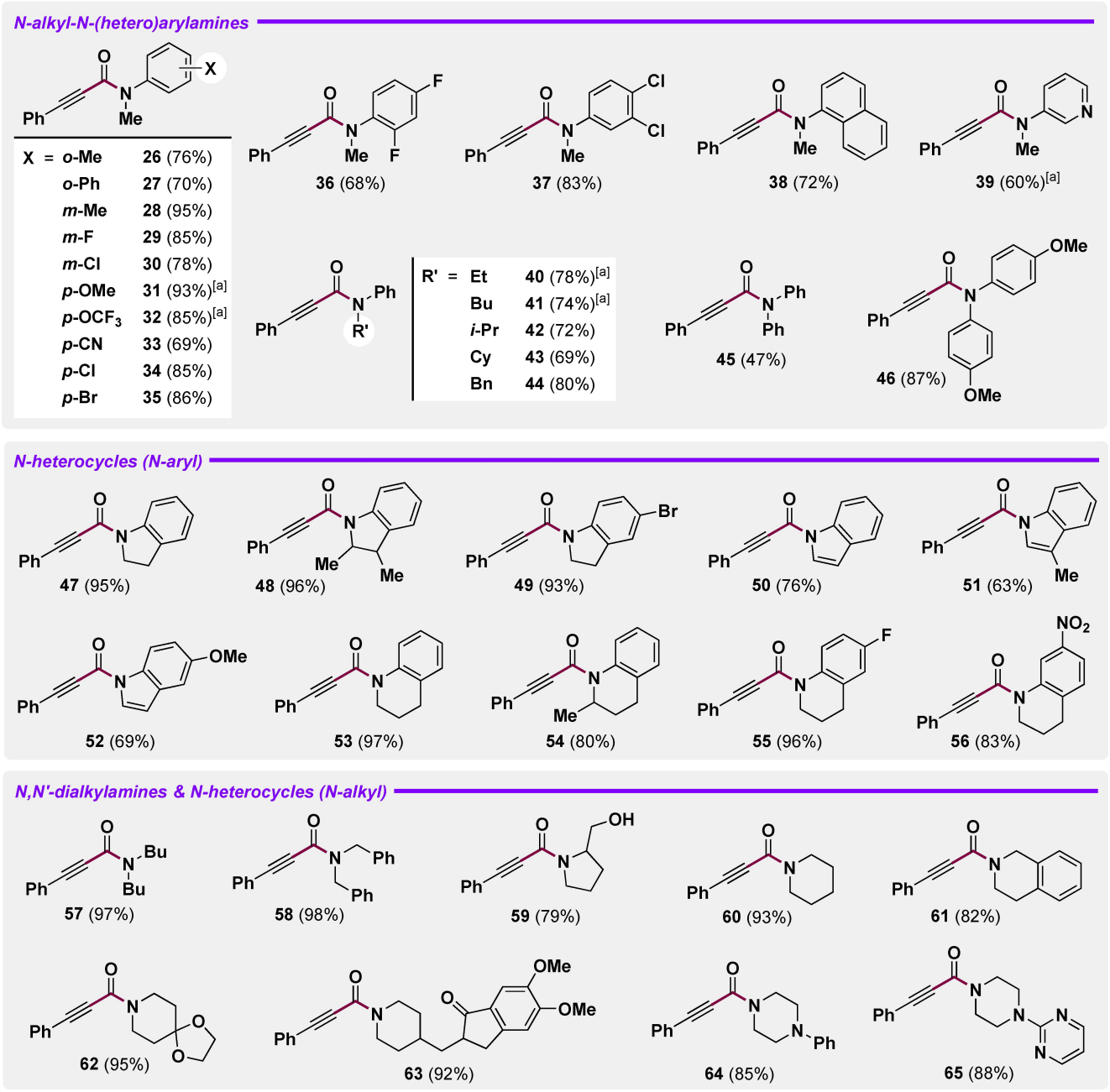

Scheme 3. [Pd/Mg_3Al-LDH]-300(D)-catalyzed oxidative aminocarbonylation of phenylacetylene **1** with (hetero)aromatic and aliphatic secondary amines and CO/O_2. Standard reaction conditions: phenylacetylene **1** (14 μL, 0.127 mmol), amine (0.19 mmol, 1.5 equiv.), [Pd/Mg_3Al-LDH]-300(D) (2.5 mol% Pd, 0.75 wt% Pd in the material, 45 mg), TBAI (5 mol%, 0.006 mmol, 2.3 mg), EtOAc (1 mL), CO/O_2 (20/5 bar) at 120 °C during 16 h (for *N*-alkyl-*N*-(het)arylamines), CO/O_2 (5/1 bar) at 80 °C during 24 h (for *N*,*N*-dialkylamines). Isolated yields after column chromatography on silica are given between parentheses. [a] Run under CO/O_2 (15/5 bar) at 80 °C during 16 h. Cy = cyclohexyl. Bn = benzyl.

Alzheimer disease treatment, and **65**, containing a structural fragment of the drug buspirinone® (Buspar) commercialized for anxiety disorders, were also obtained in very good yields.

Therefore, more than 60 substituted propiolamide derivatives were accessed by using our catalytic aminocarbonylation process (Scheme 2 and 3), being 27 of them novel molecules,

what shows the important applicability, versatility (aromatic and aliphatic can be likewise employed) and great potential of the developed methodology.

Conclusions

In conclusion, we report here the first heterogeneous reusable nanocatalyst able to selectively mediate the oxidative aminocarbonylation of alkynes with poorly nucleophilic aromatic amines in the presence of CO/O_2 mixture to afford valuable *N*-arylpropiolamides. The key of this work relies on the design of a catalytic material composed by small Pd nanoaggregates (2.8 nm average size) homogeneously distributed over a partially dehydrated LDH matrix. [Pd/Mg_3Al-LDH]-300, composed by Pd(0) and Pd(II) species, and [Pd/Mg_3Al-LDH]-300(D), containing Pd(0) species exclusively, have shown to be active materials for this transformation. Mechanistic, kinetic and characterization studies have allowed us to propose [PdI_2] species formed at the surface of the matrix support as the active centers mediating this transformation. These species are generated *in situ* in the active materials under the optimal reaction conditions employing TBAI/O_2 as oxidizing system. Under these conditions, we could elucidate that [Pd/Mg_3Al-LDH]-300(D) is the most active catalyst as it gives place more efficiently to [PdI_2] active centers catalyzing the aminocarbonylation of alkynes with high initial rates and avoiding an induction period. Moreover, a detailed characterization (XRPD, ^{27}Al MAS NMR, TGA, TPD-CO_2, BET surface area) of several [Pd/Mg_xAl-LDH] materials pyrolized at different temperatures has revealed that the use as support of a partially dehydrated LDH, with a small crystallite size, remanent interlayer water strongly bound, partially dehydroxylated and a with Mg/Al ratio of 3 gives place to a nanomaterial with the suitable acid-base properties for promoting the activation of aromatic amines in this process. In fact, this is the first reported catalyst system, either of homogeneous or heterogeneous nature, able to perform the aminocarbonylation of alkynes using aromatic amines, including *N*-aryl heterocycles and even *N,N*-diarylamines. The applicability and versatility of this nanostructured catalytic system has been demonstrated by the synthesis of more than 60 alkynamides, being 27 novel molecules, which shows the great potential of this method, also applicable to aliphatic amines. Furthermore, the stability of the most active catalysts has been proved. From our viewpoint, this work is an interesting example of application of LDH-based nanomaterials with a careful tuning of their structure and properties as catalysts in a sophisticated organic transformation, that certainly can open the door to further organic applications of this type of systems.

Experimental Section

General Information. [Mg_xAl-LDH] supports and [Pd/Mg_xAl-LDH] catalysts without thermically treatment or pyrolized under N_2 flow and/or reduced under H_2 flow or calcined under air flow, at the indicated temperature, were analyzed in powder by X-ray powder diffraction (PXRD) using a Cubix-Pro PANalytical diffractometer equipped with a detector PANalytical X'Celerator (CuK_α radiation). The wt% amount of Mg and Al in the [Mg_xAl-LDH] supports and the wt% amount of Pd contained in the fresh and used [Pd/Mg_xAl-LDH] catalysts was determined by inductively coupled plasma-atomic emission spectrometer (ICP-AES) using a Varian 715-ES after the dissolution of the solid samples in HF:HNO_3:HCl aqueous solution (1:1:3 vol). The wt% amount of carbon present in the [Mg_xAl-LDH] supports was determined by elemental analysis using a EURO EA elemental analysis equipment (Eurovector) coupled with a TCD. Thermogravimetric analysis (TGA) experiments were performed in a Netzsch STA 449 F3 Jupiter thermal analyser, using 10 mg of material and increasing the temperature from room temperature to 900 °C with a heating ramp of 10 °C/min under air flow. Liquid nitrogen adsorption was analyzed using N_2 adsorption isotherms at −196 °C in a Micromeritics FlowSorb equipment. The specific surface areas of the materials were calculated by applying the Brunauer-Emmett-Teller (BET) model over the rage $P/P^0 = 0.05$–0.25 of the isotherms. Fresh and used [Pd/Mg_3Al-LDH]-300 catalyst was observed by HRSTEM and HRTEM by using a JOEL JEM 2100F electron microscope working at 200 kV. Temperature-Programmed Reduction with H_2 (H_2-TPR) experiments were carried out in a Micromeritics Autochem 2910 equipped with a TCD detector, using 50 mg of the corresponding material, and increasing the temperature from room temperature to 900 °C with a heating ramp of 10 °C/min, under 10% H_2/Ar (vol%) and a constant flow rate of 50 ml/min. CO_2 thermo-programmed desorption (CO_2-TPD) profiles were obtained after a previous pretreatment step of the previously pyrolized [Pd/Mg_3Al-LDH]-$T_{pyr.}$ materials at the indicated temperature (100 mg with a pellet size of 0.4–0.8 nm) under a He flow from room temperature to 100 °C for 2 h, after cooling up to 50 °C, adsorption of the CO_2 was allowed at 50 °C, followed of the cleaning step using He flow in order to eliminate of the physiosorbed CO_2 and the thermo-programmed desorption was carried out by heating the samples from 50 °C to 900 °C with a heating rate of 10 °C/min. The evolved CO_2 was analyzed using a Micromeritics Autochem II equipped with a TCD detector on-line connected with an Omnistar mass spectrometer. ^{27}Al MAS NMR spectra were recorded at room temperature with a Bruker AV III HD 400 spectrometer at 104.6 MHz using a 3.2 mm probe spinning the samples at 20 kHz and 1 s as a recycle delay. $Al(NO_3)_3 \cdot 9H_2O$ was used as a secondary reference (0 ppm). The XPS spectra were recorded with a SPECS spectrometer equipped with a Phoibos 150 MCD-9 multichannel analyzer, using a non-monochromatic Mgk_α (1253.6 eV) or Alk_α (1486.6 eV) X-ray source. The spectra were recorded with an X-ray power of 100 W, pass energy of 30 eV, and under an operating pressure of 10^{-9} mbar. The XPS spectra were referenced to C1s peak (284.5 eV), and spectra treatment was performed using the CASA XPS software.

General Procedures for Materials Preparation

[Pd/Mg_3Al-LDH]-$T_{pyr.}$ ($T_{pyr.}$ = 150, 300, 400, 500 or 600 °C) materials with a 0.75 wt% of Pd were prepared by impregnation at room temperature of [Mg_3Al-LDH] support (992.5 mg) with a solution of [$Pd(acac)_2$] (21.3 mg, 0.07 mmol) in acetone (50 mL). The mixture was stirred 16 h and then evaporated to dryness under vacuum at 80 °C. The resulting powder was pyrolized at the noted temperature (150, 300, 400, 500 or 600 °C) during 3 h under N_2 flow (100 mL/min) with a heating ramp of 2 °C/min to obtain the pyrolized catalyst. [Pd/Mg_3Al-LDH]-based materials, with a 0.25, 1.5 or 3 wt% of Pd loading, were obtained following the same method but employing the required amounts of [$Pd(acac)_2$] and [Mg_3Al-LDH] in each case. For the synthesis of the corresponding [Pd/support]-500 or −300 materials with different supports, the same general procedure was followed changing the [Mg_3Al-LDH] support by

$[La_2O_3]$, [MgO], $[CeO_2]$, $[Al_2O_3]$, $[MgAl_2O_4]$, $[Mg_2Al\text{-}LDH]$, $[Mg_4Al\text{-}LDH]$ and $[Mg_5Al\text{-}LDH]$, applying the indicated pyrolysis temperature (300 or 500 °C). Commercial $[La_2O_3]$, [MgO], $[CeO_2]$ and $[MgAl_2O_4]$ supports were calcined at 500 °C during 2 h under air flow (100 mL/min) with a heating ramp of 5 °C/min before their use. Dehydrated lamellar double hydroxide support [*dh*-LDH] (without Pd) was obtained by pyrolysis of commercially available $[Mg_3Al\text{-}LDH]$ support at 300 °C during 3 h under N_2 flow (100 mL/min) with a heating ramp of 2 °C/min. $[Pd/Mg_3Al\text{-}LDH]$-300(A) material with a 0.75 wt% of Pd was prepared by impregnation at room temperature of a previously pyrolized $[Mg_3Al\text{-}LDH]$ support (at 300 °C, N_2 flow, 2 °C/min) (992.5 mg) with a solution of $[Pd(acac)_2]$ (21.3 mg, 0.07 mmol) in acetone (50 mL). The mixture was stirred 16 h and then evaporated to dryness under vacuum at 80 °C. The resulting powder was pyrolized at 300 °C during 3 h under N_2 flow (100 mL/min) with a heating ramp of 2 °C/min to obtain the pyrolized catalyst. $[Pd/Mg_3Al\text{-}LDH]$-300(B), $[Pd/Mg_3Al\text{-}LDH]$-300(C) and $[Pd/Mg_3Al\text{-}LDH]$-300(D) materials were synthetized as the above-mentioned $[Pd/Mg_3Al\text{-}LDH]$-300 material but with modifications in the thermically treatment step applied to the just impregnated $[Pd/Mg_3Al\text{-}LDH]$ catalyst as follows: $[Pd/Mg_3Al\text{-}LDH]$-300(B) was obtained after calcination under air flow (100 mL/min) at 300 °C during 3 h with a heating ramp of 2 °C/min, $[Pd/Mg_3Al\text{-}LDH]$-300(C) was obtained after reduction under H_2 flow (100 mL/min) at 300 °C during 3 h with a heating ramp of 2 °C/min and $[Pd/Mg_3Al\text{-}LDH]$-300(D) was obtained after pyrolysis under N_2 flow (100 mL/min) at 300 °C during 3 h with a heating ramp of 2 °C/min followed by reduction under H_2 flow (100 mL/min) at 200 °C during 3 h with a heating ramp of 2 °C/min.

General Catalytic Procedures

General procedure for the catalytic studies in the heterogeneously Pd-catalyzed oxidative aminocarbonylation of phenylacetylene (1) with *N*-methylaniline (2) and CO/O_2 mixture. A 8 mL glass vial containing a stirring bar was sequentially charged with phenylacetylene **1** (14 μl, 0.127 mmol), *N*-methylaniline **2** (21 μL, 0.19 mmol, 1.5 equiv.), $[Pd/Mg_3Al\text{-}LDH]\text{-}T_{pyr}$. (1, 1.5 or 2.5 mol% Pd, 0.25 to 3 wt% Pd in the material), TBAI (2.5 or 5 mol%), *n*-hexadecane (19.3 mg, 0.09 mmol) as internal standard and EtOAc (1 mL) as solvent under air atmosphere. Afterwards, the reaction vial was capped with a septum equipped with a syringe and set in the alloy plate, which was then placed into a 300 mL autoclave. Once sealed, the autoclave was purged once with 5 bar of O_2, then pressurized with 5 bar of O_2 and 15 bar of CO (final pressure 20 bar at room temperature) and placed into an aluminium block, which was preheated at 60, 80 or 100 °C. After 4 or 16 h at the indicated temperature, the autoclave was cooled in an ice bath, and the remaining gas was carefully released. Finally, the reaction mixture was diluted with ethyl acetate and analysed by GC.

General procedure for the synthesis of *N*,3-propiolamides via $[Pd/Mg_3Al\text{-}LDH]$-300(D)-catalyzed oxidative aminocarbonylation of alkynes with amines and CO/O_2 mixture. A 8 mL glass vial containing a stirring bar was sequentially charged with the corresponding alkyne (0.127 mmol), amine (0.19 mmol, 1.5 equiv.), $[Pd/Mg_3Al\text{-}LDH]$-300(D) (2.5 mol% Pd, 0.75 wt% Pd in the material, 45 mg), TBAI (5 mol%, 0.006 mmol, 2.3 mg), *n*-hexadecane (19.3 mg, 0.09 mmol) as internal standard and EtOAc (1 mL) as solvent under air atmosphere. Afterwards, the reaction vial was capped with a septum equipped with a syringe and set in the alloy plate, which was then placed into a 300 mL autoclave. Once sealed, the autoclave was purged once with 5 bar of O_2, then pressurized with O_2 (1 or 5 bar) and CO (5, 15 or 20 bar) (final pressure 6, 20 or 25 bar at room temperature) and placed into an aluminium block, which was preheated at 80 or 120 °C. After 16 or 24 h at the indicated temperature, the autoclave was cooled in an ice bath, and the remaining gas was carefully released. Finally, the reaction mixture was diluted with ethyl acetate, centrifuged and the supernatant was analysed by GC. Then, the solvent was evaporated at reduced pressure and the crude of the reaction was purified by silica gel column chromatography (*n*-hexane/EtOAc) to give the desired product.

Supporting Information

Additional experimental procedures, additional catalytic experiments, compounds and materials characterization data are included. The authors have cited additional references within the Supporting Information.[85–91]

Acknowledgements

This work was supported by Generalitat Valenciana with SEJI program (Subvencions Excelencia Juniors Investigadors, grants SEJI/2019/006 and SEJI/2020/013) and PROMETEO/2021/077, RETOS I+D+I program from MICINN (PID2019-109656RA-I0 / AEI / 10.13039/501100011033) and a program from "La Caixa" Foundation (ID 100010434), fellowship code LCF/BQ/PI18/11630023. J. R. C.-A. and R. A. thank to MICINN (Spanish Government) for two Ramón y Cajal contracts (ref. RYC-2017-22717 and RYC2020-029493-I). The authors thank Dr. María Cabrero-Antonino and Prof Rafael Ballesteros for fruitful discussions, and Luis Izquierdo-Aranda for his valuable help with LDH supports. The authors also acknowledge support of the publication fee by the CSIC Open Access Publication Support Initiative through its Unit of Information Resources for Research (URICI). A special acknowledgement is expressed to Katya Cuevas for performing the artwork in the inside cover.

Conflict of Interests

The authors declare no conflict of interest.

Data Availability Statement

The data that support the findings of this study are available in the supplementary material of this article.

Keywords: Heterogeneous Catalysis · Oxidative aminocarbonylation · Alkynes · Propiolamides · Organic synthesis

[1] C. Liu, H. Zhang, W. Shi, A. Lei, *Chem. Rev.* **2011**, *111*, 1780–1824.
[2] W. Shi, C. Liu, A. Lei, *Chem. Soc. Rev.* **2011**, *40*, 2761–2776.
[3] C. Liu, J. Yuan, M. Gao, S. Tang, W. Li, R. Shi, A. Lei, *Chem. Rev.* **2015**, *115*, 12138–12204.
[4] M. C. Kozlowski, *Acc. Chem. Res.* **2017**, *50*, 638–643.
[5] T. Dalton, T. Faber, F. Glorius, *ACS Cent. Sci.* **2021**, *7*, 245–261.

[6] Q. Liu, H. Zhang, A. Lei, *Angew. Chem. Int. Ed.* **2011**, *50*, 10788–10799.
[7] X. F. Wu, H. Neumann, M. Beller, *ChemSusChem* **2013**, *6*, 229–241.
[8] Y. Liu, Y. H. Chen, H. Yi, A. Lei, *ACS Catal.* **2022**, *12*, 7470–7485.
[9] A. N. Campbell, S. S. Stahl, *Acc. Chem. Res.* **2012**, *45*, 851–863.
[10] N. Senn, M. Ott, J. Lanz, R. Riedl, *J. Med. Chem.* **2017**, *60*, 9585–9598.
[11] J. C. Henise, J. Taunton, *J. Med. Chem.* **2011**, *54*, 4133–4146.
[12] O. Jackowski, J. Wang, X. Xie, T. Ayad, Z. Zhang, V. Ratovelomanana-Vidal, *Org. Lett.* **2012**, *14*, 4006–4009.
[13] W. C. Gao, T. Liu, Y. F. Cheng, H. H. Chang, X. Li, R. Zhou, W. L. Wei, Y. Qiao, *J. Org. Chem.* **2017**, *82*, 13459–13467.
[14] H. Yokoe, A. Kiriyama, M. Shimoda, S. Nakajima, Y. Hashizume, Y. Endo, R. Iwamoto, M. Tsubuki, N. Kanoh, *J. Org. Chem.* **2023**, *88*, 1803–1814.
[15] P. A. Donets, E. V. Van Der Eycken, *Org. Lett.* **2007**, *9*, 3017–3020.
[16] B. Gabriele, P. Plastina, G. Salerno, R. Mancuso, M. Costa, *Org. Lett.* **2007**, *9*, 3319–3322.
[17] A. Pinto, L. Neuville, J. Zhu, A. Pinto, L. Neuville, J. Zhu, *Angew. Chem. Int. Ed.* **2007**, *46*, 3291–3295.
[18] L. F. Yu, Y. Y. Li, M. B. Su, M. Zhang, W. Zhang, L. N. Zhang, T. Pang, R. T. Zhang, B. Liu, J. Y. Li, J. Li, F. J. Nan, *ACS Med. Chem. Lett.* **2013**, *4*, 475–480.
[19] M. X. Bi, S. Liu, Y. Huang, X. H. Xu, F. L. Qing, *Beilstein J. Org. Chem.* **2020**, *16*, 657–662.
[20] H. Hoberg, H. J. Riegel, *J. Organomet. Chem.* **1983**, *241*, 245–250.
[21] D. Qian, J. Zhang, *Chem. Commun.* **2012**, *48*, 7082–7084.
[22] J. D. Goodreid, P. A. Duspara, C. Bosch, R. A. Batey, *J. Org. Chem.* **2014**, *79*, 943–954.
[23] G. Rong, D. Liu, H. Yan, J. Chen, Y. Zheng, G. Zhang, J. Mao, *Adv. Synth. Catal.* **2015**, *357*, 71–76.
[24] L. Hu, S. Xu, Z. Zhao, Y. Yang, Z. Peng, M. Yang, C. Wang, J. Zhao, *J. Am. Chem. Soc.* **2016**, *138*, 13135–13138.
[25] J. R. Zhang, Y. Y. Liao, J. C. Deng, Z. L. Tang, Y. L. Xu, L. Xu, R. Y. Tang, *Asian J. Org. Chem.* **2017**, *6*, 305–312.
[26] G. F. Zha, W. Y. Fang, Y. G. Li, J. Leng, X. Chen, H. L. Qin, *J. Am. Chem. Soc.* **2018**, *140*, 17666–17673.
[27] L. Duan, K. Jiang, H. Zhu, B. Yin, *Org. Biomol. Chem.* **2021**, *19*, 365–369.
[28] Y. Tohda, K. Sonogashira, N. Hagihara, *Synthesis* **1977**, *1977*, 777–778.
[29] Y. X. Xie, R. J. Song, X. H. Yang, J. N. Xiang, J. H. Li, *Eur. J. Org. Chem.* **2013**, *2013*, 5737–5742.
[30] H. Wang, L. N. Guo, S. Wang, X. H. Duan, *Org. Lett.* **2015**, *17*, 3054–3057.
[31] J. J. Wu, Y. Li, H. Y. Zhou, A. H. Wen, C. C. Lun, S. Y. Yao, Z. Ke, B. H. Ye, *ACS Catal.* **2016**, *6*, 1263–1267.
[32] L. Wang, J. Qiu, B. Zhang, M. Chen, H. Wang, X. Miao, Z. Wu, M. Zhao, H. Shen, M. Lai, X. Shi, *ACS Omega* **2023**, *8*, 7699–7713.
[33] S. Cho, Y. Lee, K. Lee, H. Lee, Y. Lee, B. Jung, *Org. Biomol. Chem.* **2022**, *20*, 139–151.
[34] R. Zhang, Z. Y. Gu, S. Y. Wang, S. J. Ji, *Org. Lett.* **2018**, *20*, 5510–5514.
[35] P. Salehi, M. Shiri, *Adv. Synth. Catal.* **2019**, *361*, 118–125.
[36] H. Huang, G. Zhang, Y. Chen, *Angew. Chem. Int. Ed.* **2015**, *54*, 7872–7876.
[37] K. Jia, Y. Pan, Y. Chen, *Angew. Chem. Int. Ed.* **2017**, *56*, 2478–2481.
[38] P. Das, H. M. Begam, S. K. Bhunia, R. Jana, *Adv. Synth. Catal.* **2019**, *361*, 4048–4054.
[39] M. Bhargava Reddy, N. Neerathilingam, R. Anandhan, *Org. Chem. Front.* **2021**, *8*, 87–93.
[40] J. Hwang, J. Choi, K. Park, W. Kim, K. H. Song, S. Lee, *Eur. J. Org. Chem.* **2015**, *2015*, 2235–2243.
[41] Y. Dong, S. Sun, F. Yang, Y. Zhu, W. Zhu, H. Qiao, Y. Wu, Y. Wu, *Org. Chem. Front.* **2016**, *3*, 720–724.
[42] P. Szuroczki, B. Boros, L. Kollár, *Tetrahedron* **2018**, *74*, 6129–6136.
[43] B. Gabriele, G. Salerno, L. Veltri, M. Costa, *J. Organomet. Chem.* **2001**, *622*, 84–88.
[44] C. Zhang, J. Liu, C. Xia, *Catal. Sci. Technol.* **2015**, *5*, 4750–4754.
[45] N. L. Hughes, C. L. Brown, A. A. Irwin, Q. Cao, M. J. Muldoon, *ChemSusChem* **2017**, *10*, 675–680.
[46] L. Zeng, H. Li, J. Hu, D. Zhang, J. Hu, P. Peng, S. Wang, R. Shi, J. Peng, C. W. Pao, J. L. Chen, J. F. Lee, H. Zhang, Y. H. Chen, A. Lei, *Nat. Catal.* **2020**, *3*, 438–445.
[47] S. T. Gadge, M. V. Khedkar, S. R. Lanke, B. M. Bhanage, *Adv. Synth. Catal.* **2012**, *354*, 2049–2056.
[48] I. Ziccarelli, R. Mancuso, F. Giacalone, C. Calabrese, V. La Parola, A. De Salvo, N. Della Ca, M. Gruttadauria, B. Gabriele, *J. Catal.* **2022**, *413*, 1098–1110.
[49] F. Zaera, *Chem. Rev.* **2022**, *122*, 8594–8757.
[50] Z. Li, S. Ji, Y. Liu, X. Cao, S. Tian, Y. Chen, Z. Niu, Y. Li, *Chem. Rev.* **2020**, *120*, 623–682.
[51] L. Liu, A. Corma, *Chem. Rev.* **2018**, *118*, 4981–5079.
[52] M. J. Climent, A. Corma, S. Iborra, *ChemSusChem* **2009**, *2*, 500–506.
[53] S. H. Lau, P. Yu, L. Chen, C. B. Madsen-Duggan, M. J. Williams, B. P. Carrow, *J. Am. Chem. Soc.* **2020**, *142*, 20030–20039.
[54] R. Dorel, C. P. Grugel, A. M. Haydl, *Angew. Chem. Int. Ed.* **2019**, *58*, 17118–17129.
[55] A. T. Brusoe, J. F. Hartwig, *J. Am. Chem. Soc.* **2015**, *137*, 8460–8468.
[56] M. Pompeo, J. L. Farmer, R. D. J. Froese, M. G. Organ, *Angew. Chem. Int. Ed.* **2014**, *53*, 3223–3226.
[57] D. G. Evans, X. Duan, *Chem. Commun.* **2006**, 485–496.
[58] D. P. Debecker, E. M. Gaigneaux, G. Busca, *Chem. Eur. J.* **2009**, *15*, 3920–3935.
[59] G. Fan, F. Li, D. G. Evans, X. Duan, *Chem. Soc. Rev.* **2014**, *43*, 7040–7066.
[60] K. Kaneda, T. Mizugaki, *Green Chem.* **2019**, *21*, 1361–1389.
[61] J. Pérez-Ramírez, S. Abelló, N. M. Van Der Pers, *Chem. Eur. J.* **2007**, *13*, 870–878.
[62] G. R. Williams, D. O'Hare, *J. Mater. Chem.* **2006**, *16*, 3065–3074.
[63] M. Xu, M. Wei, *Adv. Funct. Mater.* **2018**, *28*, 1–20.
[64] U. A. Mohanty, D. P. Sahoo, L. Paramanik, K. Parida, *Sustain. Energy Fuels* **2023**, *7*, 1145–1186.
[65] R. D. Hetterley, R. Mackey, J. T. A. Jones, Y. Z. Khimyak, A. M. Fogg, I. V. Kozhevnikov, *J. Catal.* **2008**, *258*, 250–255.
[66] T. Mitsudome, A. Noujima, T. Mizugaki, K. Jitsukawa, K. Kaneda, *Chem. Commun.* **2012**, *48*, 11733–11735.
[67] A. Noujima, T. Mitsudome, T. Mizugaki, K. Jitsukawa, K. Kaneda, *Green Chem.* **2013**, *15*, 608–611.
[68] L. Izquierdo-Aranda, R. Adam, J. R. Cabrero-Antonino, *ChemSusChem* **2023**, *16*, e202300818.
[69] B. Gabriele, M. Costa, G. Salerno, G. P. Chiusoli, *J. Chem. Soc. Perkin Trans. 1* **1994**, 83–87.
[70] S. S. Stahl, *Angew. Chem. Int. Ed.* **2004**, *43*, 3400–3420.
[71] F. Ferretti, E. Barraco, C. Gatti, D. R. Ramadan, F. Ragaini, *J. Catal.* **2019**, *369*, 257–266.
[72] S. Kondo, K. Takizawa, A. Takahashi, K. Tokuhashi, *J. Hazard. Mater.* **2011**, *187*, 585–590.
[73] G. M. Lari, G. Pastore, C. Mondelli, J. Pérez-Ramírez, *Green Chem.* **2018**, *20*, 148–159.
[74] M. Vucelic, G. D. Moggridge, W. Jones, *J. Phys. Chem.* **1995**, *99*, 8328–8337.
[75] F. Cavani, F. Trifiro, A. Vaccari, *Catal. Today* **1991**, *11*, 173–301.
[76] R. M. Navarro, R. Guil-Lopez, J. L. G. Fierro, N. Mota, S. Jiménez, P. Pizarro, J. M. Coronado, D. P. Serrano, *J. Anal. Appl. Pyrolysis* **2018**, *134*, 362–370.
[77] Z. Ren, Y. Yang, S. Wang, X. Li, H. Feng, L. Wang, Y. Li, X. Zhang, M. Wei, *Appl. Catal. B.* **2021**, *295*, 120290–120290.
[78] J. Li, Q. Wang, S. Yu, Z. Wei, H. Zhang, *ACS Sustainable Chem. Eng.* **2022**, *10*, 7223–7233.
[79] J. A. van Bokhoven, J. C. A. A. Roelofs, K. P. de Jong, D. C. Koningsberger, *Chem. Eur. J.* **2001**, *7*, 1258–1265.
[80] W. Yang, Y. Kim, P. K. T. Liu, M. Sahimi, T. T. Tsotsis, *Chem. Eng. Sci.* **2002**, *57*, 2945–2953.
[81] J. Rocha, M. del Arco, V. Rives, M. A. Ulibarri, *J. Mater. Chem.* **1999**, *9*, 2499–2503.
[82] P. Claus, H. Berndt, C. Mohr, J. Radnik, E. J. Shin, M. A. Keane, *J. Catal.* **2000**, *192*, 88–97.
[83] I. Kovács, F. Solymosi, *J. Phys. Chem.* **1993**, *97*, 11056–11063.
[84] D. Wu, W. Y. Hernández, S. Zhang, E. I. Vovk, X. Zhou, Y. Yang, A. Y. Khodakov, V. V. Ordomsky, *ACS Catal.* **2019**, *9*, 2940–2948.
[85] D. X. Hu, P. Grice, S. V. Ley, *J. Org. Chem.* **2012**, *77*, 5198–5202.
[86] M.-B. Zhou, W.-T. Wei, Y.-X. Xie, Y. Lei, J.-H. Li, *J. Org. Chem.* **2010**, *75*, 5635–5642.
[87] H.-L. Hua, Y.-T. He, Y.-F. Qiu, Y.-X. Li, B. Song, P. Gao, X.-R. Song, D.-H. Guo, X.-Y. Liu, Y.-M. Liang, *Chem. Eur. J.* **2015**, *21*, 1468–1473.
[88] J.-S. Tang, Y.-X. Xie, Z.-Q. Wang, J.-H. Li, *Synthesis* **2011**, *2011*, 2789–2795.
[89] Y. Zhou, X. Zhang, Y. Zhang, L. Ruan, J. Zhang, D. Zhang-Negrerie, Y. Du, *Org. Lett.* **2017**, *19*, 150–153.
[90] C.-S. Wang, T. Roisnel, P. H. Dixneuf, J.-F. Soulé, *Adv. Synth. Catal.* **2019**, *361*, 445–450.
[91] R.-J. Song, Y. Liu, R.-J. Li, J.-H. Li, *Tetrahedron Lett.* **2009**, *50*, 3912–3916.

Manuscript received: February 16, 2024
Revised manuscript received: April 15, 2024
Accepted manuscript online: May 2, 2024
Version of record online: June 11, 2024